

Singularity Distance Computations for 3-RPR Manipulators using Extrinsic Metrics

Aditya Kapilavai and Georg Nawratil

*Institute of Discrete Mathematics and Geometry & Center for Geometry and Computational Design, TU Wien
Wiedner Hauptstrasse 8–10, Vienna 1040, Austria*

Abstract

It is well-known that parallel manipulators are prone to singularities. There is still a lack of distance evaluation functions, referred to as metrics, for computing the distance between two 3-RPR configurations. The presented extrinsic metrics take the combinatorial structure of the manipulator into account as well as different design options. Using these extrinsic metrics, we formulate constrained optimization problems, which aim to find the closest singular configurations for a given non-singular configuration. The solution of the corresponding system of polynomial equations relies on algorithms from numerical algebraic geometry implemented in the software package *Bertini*. Moreover, we developed a computational pipeline for computing the singularity distance along a 1-parametric motion of the manipulator. To facilitate these computations for the user, an open-source interface is developed between software packages *Maple*, *Bertini*, and *Paramotopy*. The presented approach is demonstrated based on a numerical example.

Keywords: 3-RPR planar parallel manipulator, singularity distance, extrinsic metric, numerical homotopy continuation, constrained optimization

1. Introduction

A 3-RPR manipulator (cf. Fig. 1) is a three Degree-of-Freedom (DoF) planar parallel manipulator with two translational DoFs and one rotational DoF. The base and platform are connected by three legs, where each leg consists of two passive revolute (R) joints connected by an actuated prismatic (P) joint (cf. Fig. 1). Note that we will not consider any motion range limitations on P and R joints.

Let \mathbf{k}_i denote the coordinate vectors of the base anchor points with respect to the fixed frame with coordinates $(x_i, y_i)^T$ for $i = 1, 2, 3$. The coordinate vectors of the platform anchor points with respect to the moving frame are \mathbf{p}_j with coordinates $(x_j, y_j)^T$ for $j = 4, 5, 6$. Their coordinate vectors with respect to the fixed frame can be computed as:

$$\mathbf{k}_j = \mathbf{R}\mathbf{p}_j + \mathbf{t} \quad (1)$$

*Corresponding author: Aditya Kapilavai

Email address: {akapilavai, nawratil}@geometrie.tuwien.ac.at (Aditya Kapilavai and Georg Nawratil)

where \mathbf{R} is a 2×2 rotation matrix and \mathbf{t} is the translation vector.

Without loss of generality, we can assume that \mathbf{k}_1 is the origin of the fixed frame ($\Rightarrow x_1 = y_1 = 0$) and \mathbf{k}_2 is located on the x -axis of the fixed frame ($\Rightarrow y_2 = 0$). The same assumptions can be made for the moving frame which implies $x_4 = y_4 = y_5 = 0$. The remaining six coordinates $x_2, x_3, y_3, x_5, x_6, y_6$ can be seen as the design parameters of the base and platform, respectively.

In the remainder of the paper, we denote a 3-RPR configuration by \mathbf{K} with $\mathbf{K} := (\mathbf{k}_1, \dots, \mathbf{k}_6)$.

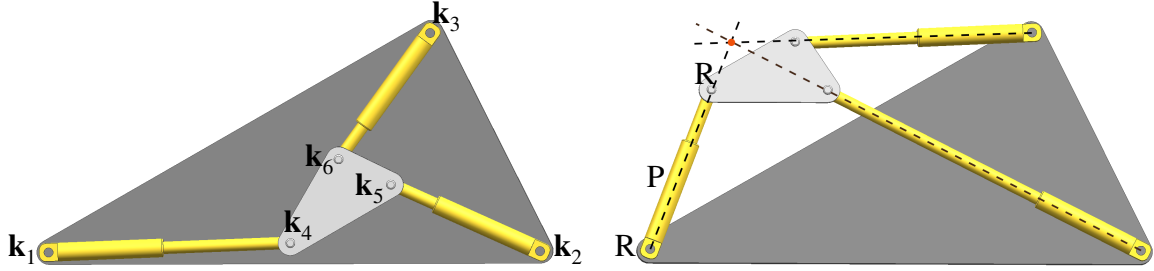


Figure 1: (left) 3-RPR planar parallel manipulator with base anchor points $\mathbf{k}_1, \mathbf{k}_2, \mathbf{k}_3$ and platform anchor points $\mathbf{k}_4, \mathbf{k}_5, \mathbf{k}_6$, where \mathbf{k}_i denotes the coordinate vector of the i th attachment with respect to the fixed frame. (right) Singular configuration of a 3-RPR manipulator.

The 3-RPR manipulator is the best-studied planar parallel mechanism, and their singularities are well understood from various points of view (e.g. [1]). It is well known that 3-RPR manipulators have at least one uncontrollable instantaneous DoF in singular (also known as shaky or infinitesimal flexible) configurations. Moreover in their neighborhood, minor geometry variations caused by, e.g., backlash in the joints and uncertainties in the actuation of P-joints, respectively, can significantly affect the resulting manipulator pose. Another phenomenon that appears close to singularities is that the actuator forces can become very large, which may result in a breakdown of the manipulator [2]. Therefore, singularities and their vicinities should be avoided, which reasons the interest of the kinematic/robotic community in evaluating the singularity closeness. Even though a lot of performance indices are given in the literature, which can also be seen as closeness indices to singularities, there is still a lack of such distance metrics, where one can distinguish the following two kinds:

1. Intrinsic metrics: The distance to the singularity is measured based on the inner metric of the manipulator, which is determined by the distances ℓ_{ij} between \mathbf{k}_i and \mathbf{k}_j with $i < j$ and $(i, j) \in \{(1, 2), (2, 3), (1, 3), (1, 4), (2, 5), (3, 6), (4, 5), (5, 6), (4, 6)\}$. Singularity distance computations for 3-RPR manipulators using intrinsic metrics is presented by the authors in [3].
2. Extrinsic metrics: The distance to the singularity is measured based on the metric of the embedding space of the manipulator, which is in our case the Euclidean plane \mathbb{R}^2 . The resulting singularity distance also implies the radius of singularity-free spheres in the configuration space, which can e.g. be used for path-planning [4].

1.1. Review on extrinsic singularity distance computations

Since the early days of robotics numerous *kinematic performance indices*¹ have been defined. As a 3-RPR robot cannot transmit the motion standstill of the P-joints to the moving platform within a singular configuration, kinematic performance indices are also sometimes regarded as *closeness indices* to singularities. As a complete review of all these closeness indices is out of the scope of this paper, we only discuss those that identify the closest singular configuration to a given non-singular one.

- Li et al [6] determined a singularity-free zone around a non-singular configuration as follows: They parameterized the 3-dimensional configuration space by x, y, ζ , where x, y are the two position variables and ζ the orientation angle. Then point (x, y, ζ) of the singularity variety which minimizes the function

$$d = (x - x_0)^2 + (y - y_0)^2, \quad (2)$$

where $(x_0, y_0)^T$ corresponds to the position of the given non-singular configuration. Note that the orientation of the given configuration is not taken into account thus \sqrt{d} is the radius of the circular directrix centered in $(x_0, y_0)^T$ of the “*singularity-free cylinder*”. This concept was also used in [7].

- The second author presented in [8, Eq. (3)] the following extrinsic metric to compute the distance between two configurations \mathbf{K} and \mathbf{K}' :

$$D^*(\mathbf{K}, \mathbf{K}')^2 = \frac{1}{6} \sum_{i=1}^6 \|\mathbf{k}'_i - \mathbf{k}_i\|^2. \quad (3)$$

The upper and lower bullets in Eq. (3) indicate that the distance is measured between corresponding platform and base anchor points of the two configurations. This preliminary extrinsic metric was already used for determining the singularity distance, which has the following physical interpretation according to [8, Theorem 1]: *If the radial clearance of the six passive R-joints is smaller than D^* , then the parallel manipulator is guaranteed to be not in a singular configuration.* More details on the performed singularity distance computation are summarized in the next subsection.

1.2. Singularity distance computation using the preliminary extrinsic metric

From the line-geometric point of view a 3-RPR configuration \mathbf{K}' is singular if and only if the carrier lines of the three legs intersect in a common point (cf. Fig. 1) or are parallel. This is equivalent to the fact that the Plücker coordinates of these lines are linearly dependent, which results in the algebraic characterization in form of the so-called *singularity variety* $V = 0$ with

$$V = \det \mathbf{J}, \quad \mathbf{J} := \begin{pmatrix} \mathbf{k}'_4 - \mathbf{k}'_1 & \mathbf{k}'_5 - \mathbf{k}'_2 & \mathbf{k}'_6 - \mathbf{k}'_3 \\ \det(\mathbf{k}'_1, \mathbf{k}'_4 - \mathbf{k}'_1) & \det(\mathbf{k}'_2, \mathbf{k}'_5 - \mathbf{k}'_2) & \det(\mathbf{k}'_3, \mathbf{k}'_6 - \mathbf{k}'_3) \end{pmatrix}. \quad (4)$$

¹A kinematic performance index of a robotic mechanical system converts the capability of the system to transmit motions (at the level of velocities) into a scalar (cf.[5, page 171])

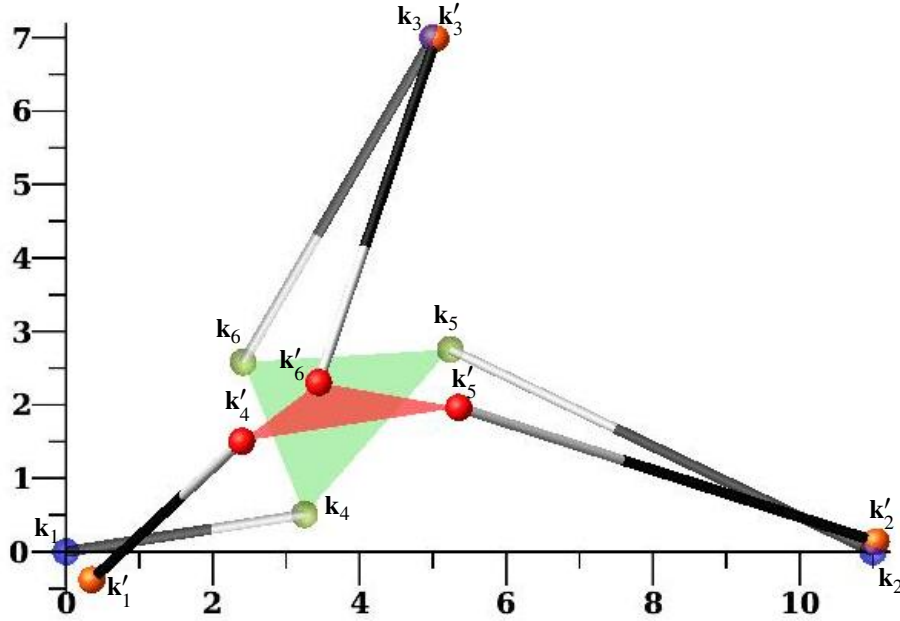


Figure 2: Closest singular configuration \mathbf{K}' (red) for a given non-singular 3-RPR manipulator pose \mathbf{K} (green) with $D^*(\mathbf{K}, \mathbf{K}') = 0.7541454$ units. \mathbf{K} corresponds to the configuration given in [8, Section 3] for $\phi = 0.8471710528$ radians.

The *singularity polynomial* V is of degree 4 in the coordinates $(c_i, d_i)^T$ of the points \mathbf{k}'_i with respect to the fixed frame (for $i = 1, \dots, 6$).

The minimization of $D^*(\mathbf{K}, \mathbf{K}')$ given in Eq. (3) under the side condition $V = 0$ of Eq. (4) is a constrained optimization problem, which can be formulated as the Lagrange function L with

$$L = D^*(\mathbf{K}, \mathbf{K}')^2 + \lambda V, \quad (5)$$

where λ is the Lagrange multiplier.

To find the closest singular configuration, one needs to compute the critical points of L as the zero sets of the partial derivatives of L with respect to the involved 13 unknowns $c_1, \dots, c_6, d_1, \dots, d_6$ and λ . In [8] the resulting square systems of polynomial equations were solved by using symbolic computations (Göberner basis methods) implemented in a computer algebraic system (software Maple). Then the configuration, which corresponds to the critical point causing the smallest value for $D^*(\mathbf{K}, \mathbf{K}')$, has been assigned as the closest singular configuration (cf. Fig. 2).

1.3. Motivation and outline

A limitation of the approach presented in [8] concerns the computational efficiency caused by Gröbner base calculations. As we aim to compute the singularity distance (incl. the closest singularity) along a 1-parametric motion of the manipulator, we use the numerical algebraic geometry tool of homotopy continuation implemented in the freeware Bertini [9]. To facilitate these computations for the user, an open-source interface is developed between the software packages Maple, Bertini [10], and Paramotopy [11].

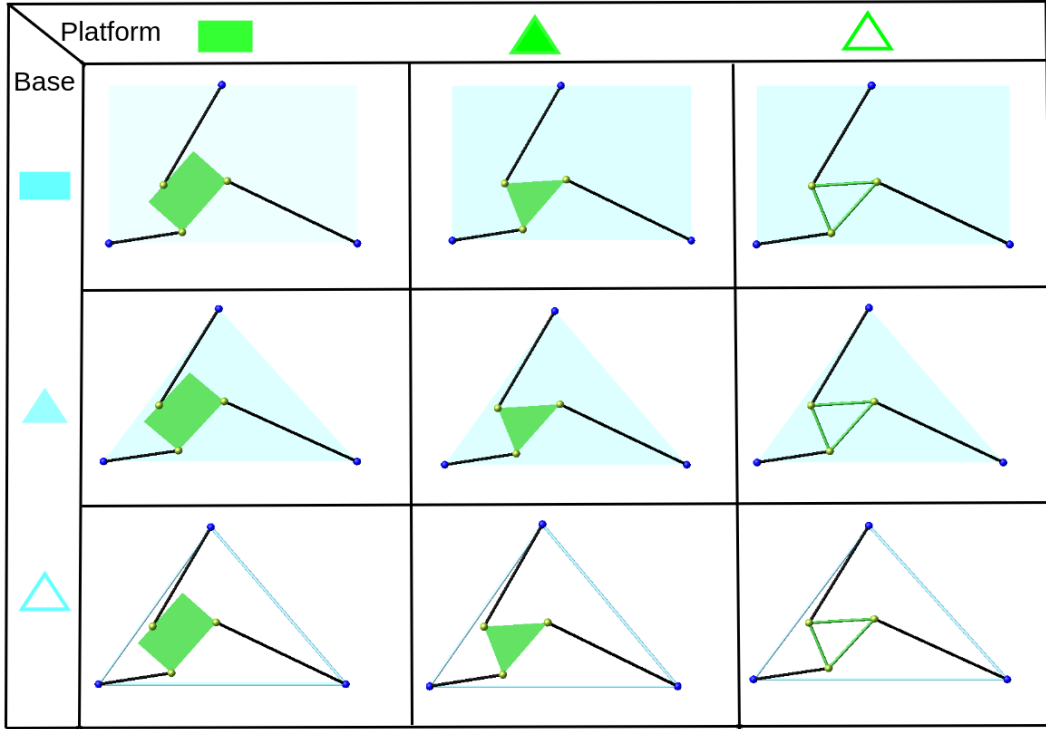


Figure 3: An illustration of the nine considered interpretations of 3-RPR manipulators arranged in a 3×3 matrix.

Moreover, the paper at hand also fills the gap that singular points of the singular variety $V = 0$ are excluded from the Lagrangian approach given in Eq. (5) as pointed out in [4, Section 3.2.2]. We identify these points, which are considered separately within the presented computational pipeline.

A further limitation of the distance metric D^* given in Eq. (3) is that it does not take into account how the six anchor points are connected combinatorially. Especially for the three platform/base anchor points one can distinguish two basic design options; namely if they are considered as the vertices of a triangular plate (\blacktriangle) or as the pin-joints of a triangular bar structure (\triangle). Note that in the latter case, additional shaky configurations arise by the collinearity of the three base/platform points.

In the general case, the structural components (bars and plates) are assumed to be made of deformable material allowing not only a variation of the leg lengths² but also a change of the platform/base geometry by an affine transformation. We also take the option into account that the platform/base is made of a non-deformable material, which is indicated by the symbol \blacksquare , restricting affine transformations to Euclidean motions. Thus we end up with three possibilities (\blacktriangle , \triangle , \blacksquare) for the platform/base, which results in a total of nine interpretations illustrated in Fig. 3.

Remark 1. Note that we have distinguished the same nine interpretations in the already mentioned study [3] using intrinsic metrics. In the paper at hand, we present the corresponding extrinsic

²Note that the legs are also considered as bars.

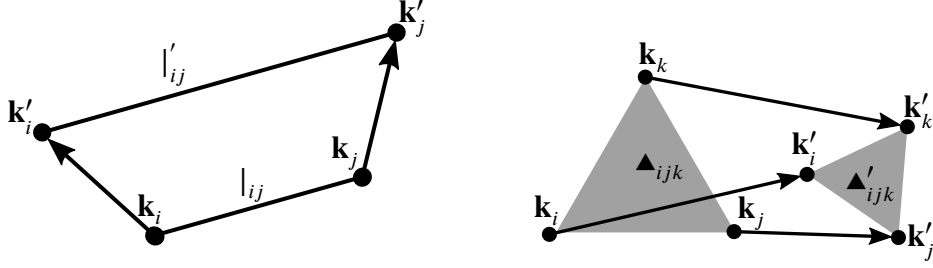


Figure 4: (left) Similarity mapping between line-segments. (right) Affine mapping between triangles.

metrics. These paired intrinsic and extrinsic metrics can be used for quantifying the change in the shape of the manipulator implied by variations of the inner geometry, which contributes to the topic of sensitivity analysis (e.g. [12]). \diamond

The combinatorial structure of the nine interpretations of Fig. 3 is taken into account by constructing extrinsic metrics, which rely on the distance computation between corresponding structural components (bars or plates) outlined in Section 2. The constrained optimization problems related to these extrinsic metrics are set up in Section 3. A geometric characterization of the singular points of the constrained varieties is obtained in Section 4. The developed computational pipeline for computing the singularity distance along a 1-parametric motion of the manipulator is given in Section 5. In Section 6 we present a numerical example and discuss the results. We conclude the paper in Section 7.

2. Extrinsic metric formulation

We start by setting up the distance function between the geometric elements (line segments and triangles) which can be associated with the structural components (bars and plates) of the manipulator.

According to [13], the squared distance between two oriented line-segments $|_{ij} = (\mathbf{k}_i, \mathbf{k}_j)$ and $|'_{ij} = (\mathbf{k}'_i, \mathbf{k}'_j)$ can be defined as (cf. Fig. 4 left):

$$d\left(|_{ij}, |'_{ij}\right)^2 = \frac{1}{3} \left[\|\mathbf{k}_i - \mathbf{k}'_i\|^2 + \|\mathbf{k}_j - \mathbf{k}'_j\|^2 + (\mathbf{k}_i - \mathbf{k}'_i)^T (\mathbf{k}_j - \mathbf{k}'_j) \right]. \quad (6)$$

This distance metric equals the square root of the mean of squared distances of corresponding³ points over the entire line segment (see also [14, Section 4.1]). One can extend this idea to compute the squared distance between two triangles $\blacktriangle_{ijk} = (\mathbf{k}_i, \mathbf{k}_j, \mathbf{k}_k)$ and $\blacktriangle'_{ijk} = (\mathbf{k}'_i, \mathbf{k}'_j, \mathbf{k}'_k)$ with $i < j < k$ (cf. Fig. 4 right) which yields (see Appendix A for the derivation)

$$d(\blacktriangle_{ijk}, \blacktriangle'_{ijk})^2 = \frac{1}{6} \left[\sum_{x=i,j,k} \|\mathbf{k}_x - \mathbf{k}'_x\|^2 + (\mathbf{k}_i - \mathbf{k}'_i)^T (\mathbf{k}_k - \mathbf{k}'_k) + (\mathbf{k}_i - \mathbf{k}'_i)^T (\mathbf{k}_j - \mathbf{k}'_j) + (\mathbf{k}_k - \mathbf{k}'_k)^T (\mathbf{k}_j - \mathbf{k}'_j) \right], \quad (7)$$

³The correspondence is given by the associated similarity transformation between $|_{ij}$ and $|'_{ij}$.

where the index set $\{i, j, k\}$ equals either $\{1, 2, 3\}$ or $\{4, 5, 6\}$. Therefore Eq. (7) equals the integral of the squared distance of corresponding⁴ points over the triangle, divided by its area.

By using Eqs. (6) and (7) the squared extrinsic distance functions $D_{\star}^{\circ}(\mathbf{K}, \mathbf{K}')^2$ with $\circ, \star \in \{\blacktriangle, \triangle, \blacksquare\}$ can be defined as the sum of the squared distances between corresponding deformable structural elements divided by the number of summands, which yields the following expressions:

$$D_{\blacksquare}^{\circ}(\mathbf{K}, \mathbf{K}') = \frac{1}{3} \sum_{(i,j) \in I_1} d(l_{ij}, l'_{ij})^2, \quad (8)$$

$$D_{\blacksquare}^{\triangle}(\mathbf{K}, \mathbf{K}') = \frac{1}{4} \left[\sum_{(i,j) \in I_1} d(l_{ij}, l'_{ij})^2 + d(\blacktriangle_{456}, \blacktriangle'_{456})^2 \right], \quad (9)$$

$$D_{\blacksquare}^{\triangle}(\mathbf{K}, \mathbf{K}') = \frac{1}{6} \sum_{(i,j) \in I_2} d(l_{ij}, l'_{ij})^2, \quad (10)$$

$$D_{\blacktriangle}^{\circ}(\mathbf{K}, \mathbf{K}') = \frac{1}{4} \left[\sum_{(i,j) \in I_1} d(l_{ij}, l'_{ij})^2 + d(\blacktriangle_{123}, \blacktriangle'_{123})^2 \right], \quad (11)$$

$$D_{\blacktriangle}^{\circ}(\mathbf{K}, \mathbf{K}') = \frac{1}{6} \sum_{(i,j) \in I_3} d(l_{ij}, l'_{ij})^2, \quad (12)$$

$$D_{\blacktriangle}^{\triangle}(\mathbf{K}, \mathbf{K}') = \frac{1}{5} \left[\sum_{(i,j) \in I_1} d(l_{ij}, l'_{ij})^2 + d(\blacktriangle_{123}, \blacktriangle'_{123})^2 + d(\blacktriangle_{456}, \blacktriangle'_{456})^2 \right], \quad (13)$$

$$D_{\blacktriangle}^{\triangle}(\mathbf{K}, \mathbf{K}') = \frac{1}{7} \left[\sum_{(i,j) \in I_2} d(l_{ij}, l'_{ij})^2 + d(\blacktriangle_{123}, \blacktriangle'_{123})^2 \right], \quad (14)$$

$$D_{\blacktriangle}^{\triangle}(\mathbf{K}, \mathbf{K}') = \frac{1}{7} \left[\sum_{(i,j) \in I_3} d(l_{ij}, l'_{ij})^2 + d(\blacktriangle_{456}, \blacktriangle'_{456})^2 \right], \quad (15)$$

$$D_{\blacktriangle}^{\triangle}(\mathbf{K}, \mathbf{K}') = \frac{1}{9} \sum_{(i,j) \in I_4} d(l_{ij}, l'_{ij})^2, \quad (16)$$

with

$$I_1 = \{(1, 4), (2, 5), (3, 6)\}, \quad (17)$$

$$I_2 = \{(1, 4), (2, 5), (3, 6), (4, 5), (4, 6), (5, 6)\}, \quad (18)$$

$$I_3 = \{(1, 4), (2, 5), (3, 6), (1, 2), (2, 3), (1, 3)\}, \quad (19)$$

$$I_4 = \{(1, 2), (2, 3), (1, 3), (1, 4), (2, 5), (3, 6), (4, 5), (5, 6), (4, 6)\}. \quad (20)$$

Note that we restrict to deformable structural components in order to keep the analogy to the corresponding intrinsic metrics mentioned in Remark 1.

⁴The correspondence is given by the associated affine transformation between \blacktriangle_{ijk} and \blacktriangle'_{ijk} .

3. The constrained optimization problem for computing the singularity distance

3.1. Closest configuration on the singularity variety

In the following, we set up the optimization problems for computing the closest singularity on the singularity variety $V = 0$ with respect to the nine extrinsic metrics presented in Section 2.

- $D_{\square}^{\square}(\mathbf{K}, \mathbf{K}')$: In this case, the transformations of the platform and the base are both restricted to the Euclidean motion group SE(2). As the so-called *point-based representation* of SE(2) has the best computational performance according to [15], we use it for our calculations. The coordinates of \mathbf{k}'_i can be given in dependence of \mathbf{k}'_{i-1} and \mathbf{k}'_{i-2} for $i = 3, 6$ by

$$\begin{pmatrix} c_3 \\ d_3 \end{pmatrix} = \begin{pmatrix} \frac{(c_2-c_1)x_3+(d_1-d_2)y_3+c_1x_2}{x_2} \\ \frac{(d_2-d_1)x_3+(c_2-c_1)y_3+d_1x_2}{x_2} \end{pmatrix}, \quad (21) \quad \begin{pmatrix} c_6 \\ d_6 \end{pmatrix} = \begin{pmatrix} \frac{(c_5-c_4)x_6+(d_4-d_5)y_6+c_4x_5}{x_5} \\ \frac{(d_5-d_4)x_6+(c_5-c_4)y_6+d_4x_5}{x_5} \end{pmatrix} \quad (22)$$

under the side condition that the distance between \mathbf{k}'_{i-1} and \mathbf{k}'_{i-2} does not change, which is expressed by the conditions $E_B = 0$ and $E_P = 0$ with

$$E_B = \|\mathbf{k}'_2 - \mathbf{k}'_1\|^2 - \|\mathbf{k}_2 - \mathbf{k}_1\|^2, \quad (23) \quad E_P = \|\mathbf{k}'_5 - \mathbf{k}'_4\|^2 - \|\mathbf{p}_5 - \mathbf{p}_4\|^2. \quad (24)$$

Note that due to Lemma 2 given in Appendix B we can always assume without loss of generality that there exists a labeling of our 3-RPR manipulator such that $x_2 \neq 0$ and $x_5 \neq 0$ hold, which is needed for the properness of Eqs. (21) and (22).

As a consequence, the Lagrange function L reads as

$$L = D_{\square}^{\square}(\mathbf{K}, \mathbf{K}')^2 + \lambda V + \mu E_B + \kappa E_P, \quad (25)$$

where λ , μ and κ are the Lagrange multipliers.

- $D_{\square}^{\circ}(\mathbf{K}, \mathbf{K}')$ with $\circ \in \{\blacktriangle, \triangle\}$: In these two cases only the base is transformed by a Euclidean displacement, thus the Lagrange function reads as:

$$L = D_{\square}^{\circ}(\mathbf{K}, \mathbf{K}')^2 + \lambda V + \mu E_B. \quad (26)$$

- $D_{\star}^{\square}(\mathbf{K}, \mathbf{K}')$ with $\star \in \{\blacktriangle, \triangle\}$: In these two cases, only the platform is transformed by a Euclidean displacement, thus the Lagrange function reads as:

$$L = D_{\star}^{\square}(\mathbf{K}, \mathbf{K}')^2 + \lambda V + \kappa E_P. \quad (27)$$

- $D_{\star}^{\circ}(\mathbf{K}, \mathbf{K}')$ with $\circ, \star \in \{\blacktriangle, \triangle\}$: In these four cases the platform, as well as the base, are transformed affinely thus the Lagrangian reads as:

$$L = D_{\star}^{\circ}(\mathbf{K}, \mathbf{K}')^2 + \lambda V. \quad (28)$$

Table 1: Summary of the Lagrange formulations of the constrained optimization problems of Sections 3.1 and 3.2

Extrinsic metric	unknowns in the Lagrangian	# unknowns
$D_{\square}^{\square}(\mathbf{K}, \mathbf{K}')$	$c_1, d_1, c_2, d_2, c_4, d_4, c_5, d_5, \lambda, \kappa, \mu$	11
$D_{\square}^{\circ}(\mathbf{K}, \mathbf{K}')$ with $\circ \in \{\blacktriangle, \triangle\}$	$c_1, d_1, c_2, d_2, c_4, d_4, c_5, d_5, c_6, d_6, \lambda, \mu$	12
$D_{\star}^{\square}(\mathbf{K}, \mathbf{K}')$ with $\star \in \{\blacktriangle, \triangle\}$	$c_1, d_1, c_2, d_2, c_3, d_3, c_4, d_4, c_5, d_5, \lambda, \kappa$	12
$D_{\star}^{\circ}(\mathbf{K}, \mathbf{K}')$ with $\circ, \star \in \{\blacktriangle, \triangle\}$	$c_1, d_1, c_2, d_2, c_3, d_3, c_4, d_4, c_5, d_5, c_6, d_6, \lambda$	13

The unknowns appearing in the given Lagrange functions L are summarized in Table 1.

As already mentioned in Section 1.3, we get additional singular configurations if the platform/base is interpreted as a triangular bar structure. The optimization problem for computing the closest configurations with collinear platform/base anchor points is discussed in the next subsection.

3.2. Closest configuration on the collinearity variety

If the base or platform is interpreted as a triangular bar-structure (Δ) the additional singularities can be characterized algebraically by the condition $C_B = 0$ and $C_P = 0$, respectively, with

$$C_B = \det \begin{pmatrix} 1 & 1 & 1 \\ c_1 & c_2 & c_3 \\ d_1 & d_2 & d_3 \end{pmatrix}, \quad C_P = \det \begin{pmatrix} 1 & 1 & 1 \\ c_4 & c_5 & c_6 \\ d_4 & d_5 & d_6 \end{pmatrix}. \quad (29)$$

Note that the so-called *collinearity varieties* $C_B = 0$ and $C_P = 0$ are quadratic in $c_1, \dots, c_6, d_1, \dots, d_6$.

In the following, we set up the optimization problems for computing the closest singularity on the collinearity variety $C_B = 0$ and $C_P = 0$, respectively.

- $D_{\square}^{\Delta}(\mathbf{K}, \mathbf{K}')$: In this case, only the platform can deform, thus the Lagrange function with collinearity condition $C_P = 0$ reads as:

$$L = D_{\square}^{\Delta}(\mathbf{K}, \mathbf{K}')^2 + \lambda C_P + \mu E_B. \quad (30)$$

- $D_{\Delta}^{\square}(\mathbf{K}, \mathbf{K}')$: In this case, only the base can deform, thus the Lagrange function with collinearity condition $C_B = 0$ reads as:

$$L = D_{\Delta}^{\square}(\mathbf{K}, \mathbf{K}')^2 + \lambda C_B + \kappa E_P. \quad (31)$$

- $D_{\star}^{\Delta}(\mathbf{K}, \mathbf{K}')$ with $\star \in \{\blacktriangle, \triangle\}$: In these two cases the platform, as well as the base, are transformed affinely thus the Lagrangian reads as:

$$L = D_{\star}^{\Delta}(\mathbf{K}, \mathbf{K}')^2 + \lambda C_P. \quad (32)$$

- $D_{\Delta}^{\circ}(\mathbf{K}, \mathbf{K}')$ with $\circ \in \{\blacktriangle, \triangle\}$: In these two cases the platform, as well as the base, are transformed affinely thus the Lagrangian reads as:

$$L = D_{\Delta}^{\circ}(\mathbf{K}, \mathbf{K}')^2 + \lambda C_B. \quad (33)$$

The number of unknowns for the Lagrange optimization problems for the mentioned above four cases either with collinearity variety $C_B = 0$ and $C_P = 0$ is the same as summarized in Table 1.

Theorem 1. *The platform anchor points of the closest configuration \mathbf{K}' on the collinearity variety $C_P = 0$ with respect to the extrinsic metric $D_\star^\Delta(\mathbf{K}, \mathbf{K}')$ with $\star \in \{\blacktriangle, \triangle\}$ are the pedal points of $\mathbf{k}_4, \mathbf{k}_5, \mathbf{k}_6$ on their line of regression (cf. Fig. 5(b) and 5(c)). Moreover, the distance $D_\star^\Delta(\mathbf{K}, \mathbf{K}')$ only depends on the geometry of the manipulator; i.e. it is pose independent.*

Proof. The partial derivatives of Eq. (32) with respect to the twelve coordinates c_i, d_i ($i = 1, \dots, 6$) and the Lagrange multiplier λ results in the following ideal of thirteen equations:

$$\mathcal{I}_1 := \langle g_1, \dots, g_{13} \rangle \subseteq \mathbb{K}[c_i, d_i, x_2, x_3, x_4, x_5, x_6, y_3, y_4, y_5, y_6, \lambda] \quad \text{for } i = 1, \dots, 6. \quad (34)$$

On the other hand, the pedal points of $\mathbf{k}_4, \mathbf{k}_5, \mathbf{k}_6$ on the line of regression can be obtained as a solution of the following optimization problem:

$$L = \frac{1}{3} \sum_{i=1}^3 \|\mathbf{k}'_i - \mathbf{k}_i\|^2 + \lambda_1 C_P \quad \text{for } i = 4, 5, 6. \quad (35)$$

The partial derivatives of Eq. (35) with respect to the six unknowns c_i, d_i ($i = 4, 5, 6$) including the multiplier λ_1 results in the following ideal:

$$\mathcal{I}_2 := \langle f_1, \dots, f_7 \rangle \subseteq \mathbb{K}[c_i, d_i, x_4, x_5, x_6, y_4, y_5, y_6, \lambda_1] \quad \text{for } i = 4, 5, 6. \quad (36)$$

In order to show that the critical points of both Lagrange formulations are identical, one can eliminate c_i, d_i, λ for $i = 1, 2, 3$ from the ideal \mathcal{I}_1 and λ_1 from \mathcal{I}_2 i.e.

$$\mathcal{I}_3 := \mathcal{I}_1 \cap \mathbb{K}[c_i, d_i, x_i, y_i, x_2, x_3, y_3], \quad \mathcal{I}_4 := \mathcal{I}_2 \cap \mathbb{K}[c_i, d_i, x_i, y_i] \quad \text{for } i = 4, 5, 6. \quad (37)$$

By the usage of the software `Maple`, it can be verified that \mathcal{I}_3 is contained in \mathcal{I}_4 and vice versa.

To prove that the distance $D_\star^\Delta(\mathbf{K}, \mathbf{K}')$ is pose independent, we parameterize the pose determined by \mathbf{R} and \mathbf{t} in Eq. (1) by

$$\mathbf{R} := \frac{1}{e_0^2 + e_1^2} \begin{pmatrix} e_0^2 - e_1^2 & -2e_0e_1 \\ 2e_0e_1 & e_0^2 - e_1^2 \end{pmatrix}, \quad \mathbf{t} := \begin{pmatrix} \alpha \\ \beta \end{pmatrix}. \quad (38)$$

Using this parametrization we take again the partial derivatives of Eq. (32) with respect to the twelve coordinates c_i, d_i ($i = 1, \dots, 6$) and the Lagrange multiplier λ . We solve the resulting system of 13 equations for λ, c_i, d_i ($i = 1, \dots, 6$) by using Gröbner basis package implemented in `Maple` and obtain two solution sets. Substituting each of the two obtained solutions for c_i, d_i ($i = 1, \dots, 6$) back into the extrinsic distance functions given by Eq. 14 and Eq. 16, respectively, shows that the resulting expression only depends on the geometry parameters x_5, x_6, y_6 . For the explicit expressions of $D_\Delta^\circ(\mathbf{K}, \mathbf{K}')$ with $\circ \in \{\blacktriangle, \triangle\}$ we refer to Appendix C.

The `Maple` files used for proving Theorem 1 can be downloaded from [16]. □

Clearly, this theorem also holds by exchanging the platform and the base which yields:

Theorem 2. *The base anchor points of the closest configuration \mathbf{K}' on the collinearity variety $C_B = 0$ with respect to the extrinsic metric $D_{\Delta}^{\circ}(\mathbf{K}, \mathbf{K}')$ with $\circ \in \{\blacktriangle, \triangle\}$ are the pedal points of $\mathbf{k}_1, \mathbf{k}_2, \mathbf{k}_3$ on their line of regression. Moreover, the distance $D_{\Delta}^{\circ}(\mathbf{K}, \mathbf{K}')$ only depends on the geometry of the manipulator; i.e. it is pose independent.*

Note that the first sentence of Theorem 1 (resp. Theorem 2) does not hold for the metric $D_{\square}^{\Delta}(\mathbf{K}, \mathbf{K}')$ (resp. $D_{\Delta}^{\square}(\mathbf{K}, \mathbf{K}')$), which is demonstrated by the following counter-example.

Counter example 1. *We use as input for our numerical example the one discussed in [8, Section 3] for $\phi = \frac{\pi}{2}$. For this configuration, we solved the optimization problems stated in Eq. (30) and Eq. (32). The configurations which correspond to the global minima are displayed in Fig. 5 and their coordinates are given in Table. 2.*

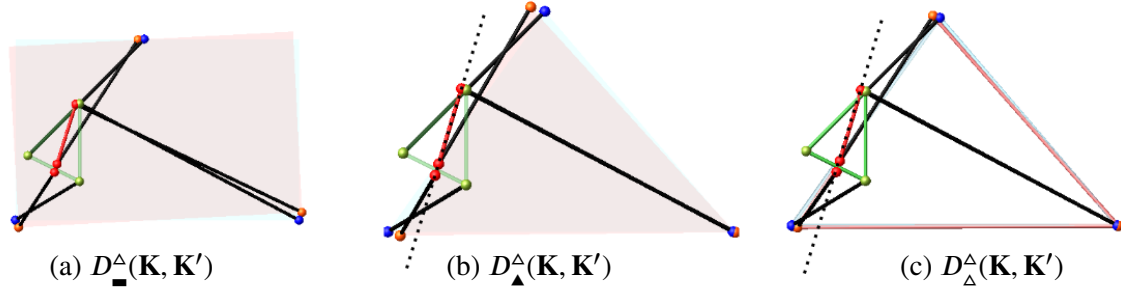


Figure 5: The line of regression is indicated by a dashed line and its equation is given by $0.9570920262x - 0.2897841482y - 0.9336136247 = 0$. From the visual point of view the platform anchor points in (a) are very similar to the ones of (b) and (c), which are identical due to Theorem 1. From Table 2 it can be seen that the coordinates of $\mathbf{k}'_4, \mathbf{k}'_5, \mathbf{k}'_6$ of (a) differ from those of (b) and (c) and that they are not fulfilling the equation of the line of regression.

Table 2: Coordinates of the closest singular configuration for counter-example 1

\mathbf{K}'	$D_{\square}^{\Delta}(\mathbf{K}, \mathbf{K}') = 0.5735791$	$D_{\Delta}^{\square}(\mathbf{K}, \mathbf{K}') = 0.5195729$	$D_{\Delta}^{\Delta}(\mathbf{K}, \mathbf{K}') = 0.46807561$
\mathbf{k}'_1	(0.1302373, -0.2775441)	(0.3921934, -0.1187466)	(0.1960967, -0.0593733)
\mathbf{k}'_2	(11.114982, 0.3015644)	(11.059373, -0.0179767)	(11.029686, -0.0089883)
\mathbf{k}'_3	(4.7547798, 6.9759796)	(4.5484332, 7.1367234)	(4.7742166, 7.0683617)
\mathbf{k}'_4	(1.5271323, 1.8504855)	(1.5195164, 1.7968665)	(1.5195164, 1.7968665)
\mathbf{k}'_5	(2.3464552, 4.4803586)	(2.3515667, 4.5449419)	(2.3515667, 4.5449419)
\mathbf{k}'_6	(1.6264123, 2.1691557)	(1.6289168, 2.1581914)	(1.6289168, 2.1581914)

Also the second sentence of Theorem 1 (resp. Theorem 2) does not hold for $D_{\square}^{\Delta}(\mathbf{K}, \mathbf{K}')$ (resp. $D_{\Delta}^{\square}(\mathbf{K}, \mathbf{K}')$), which can be seen from the example (cf. Fig. 11(a,d)) discussed in Section 6.

4. Singular points of the constraint varieties

As already mentioned the Lagrangian formulations given in Eqs. (25–28) and Eqs. (30–33) do not take the singular points of the constraint varieties into account. Therefore we have to take care of them separately, which is done in the following two subsections:

4.1. Singular points of the singularity variety

We are interested in giving a geometric characterization of the singular points of the singularity variety $V = 0$. As a preparatory work towards this goal, we prove the following lemma:

Lemma 1. *The set of singular points of the singularity variety $V = 0$ remains invariant under equiform motions.*

Proof. From Eq. (4) it can be seen that V only depends on the free coordinates c_i, d_i ($i = 1, \dots, 6$). Partial derivatives of Eq. (4) with respect to these twelve unknowns plus the singularity polynomial V results in an overdetermined system of thirteen equations spanning the following ideal:

$$\mathcal{I} := \langle g_1, \dots, g_{13} \rangle \subseteq \mathbb{K}[c_i, d_i] \quad i = 1, \dots, 6. \quad (39)$$

Now to prove translational invariance we make the substitutions

$$c_i \mapsto c_i + \alpha, \quad d_i \mapsto d_i + \beta \quad \text{for } i = 1, \dots, 6 \quad (40)$$

in g_j ($j = 1, \dots, 13$) resulting in a new system of polynomials G_j forming the following ideal:

$$\mathcal{I}_T := \langle G_1, \dots, G_{13} \rangle \subseteq \mathbb{K}[c_i, d_i, \alpha, \beta] \quad i = 1, \dots, 6. \quad (41)$$

It can be verified by the computational algebra software `Maple` that \mathcal{I} and \mathcal{I}_T are contained in each other, thus their varieties are identical.

In the second step, we prove the invariance under stretch rotations, for which we make the substitutions

$$c_i \mapsto (e_0^2 - e_1^2)c_i - 2e_0e_1d_i, \quad d_i \mapsto 2e_0e_1c_i + (e_0^2 - e_1^2)d_i \quad \text{for } i = 1, \dots, 6 \quad (42)$$

in g_j ($j = 1, \dots, 13$) resulting in a new set of polynomials G_j forming the following ideal:

$$\mathcal{I}_R := \langle G_1, \dots, G_{13} \rangle \subseteq \mathbb{K}[c_i, d_i, e_0, e_1] \quad i = 1, \dots, 6. \quad (43)$$

Again by the usage of the software `Maple`, it can be verified that \mathcal{I} is contained in \mathcal{I}_R and vice versa. The `Maple` files used for proving Lemma 1 can be downloaded from [16]. \square

By using Lemma 1 we can prove the following theorem:

Theorem 3. *Singular points of the singularity variety $V = 0$ correspond to one of the following configurations:*

1. *Three legs of the manipulator are collinear (see Fig. 6a).*
2. *Two legs are collinear and one leg degenerates to a point (see Fig. 6b).*
3. *Two legs degenerate to points (see Fig. 6c).*
4. *One leg degenerates to a point and the carrier lines of the remaining two legs pass through that point (see Fig. 6d).*

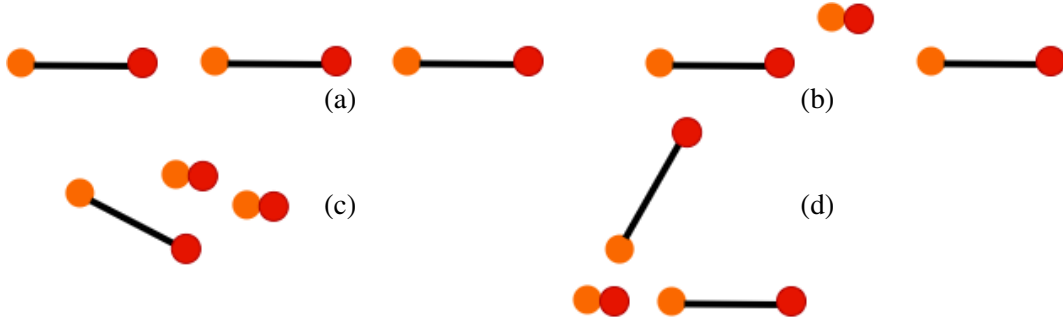


Figure 6: Schematic sketch of the geometric characterization of singular points of the singularity variety $V = 0$. Base and platform anchor points are indicated in orange and red, respectively.

Proof. Due to Lemma 1 we can set $c_1 = d_1 = d_2 = 0$ in g_i of Eq. (39) for $i = 1, \dots, 13$. This simplification allows us to solve the resulting overdetermined system in nine unknowns by using Gröbner basis method implemented in `Maple`. It can easily be checked that each of the obtained 30 solutions falls into one of the given four geometric characterization, which shows their necessity. The `Maple` file for the computation of the 30 solutions can be downloaded from [16].

The proof of sufficiency is straightforward by checking that the 13 equations of Eq. (39) are fulfilled under consideration of the listed four geometric conditions. \square

Remark 2. Note that case 4 of Theorem 3 also shows that singular points of the singularity variety are not characterized by $\text{rank}(\mathbf{J})=1$ with \mathbf{J} of Eq. (4). Therefore this also falsifies the conjecture of [17, End of Sec. IV] that singularities of the singularity variety yield higher-order singularities. \diamond

If we restrict the base (resp. platform) to be transformed by Euclidean motions, then our set of singular configurations is only a subset $V_B = 0$ (resp. $V_P = 0$) of $V = 0$.

Let us first assume that the base is transformed by Euclidean motions. Then the variety $V_B = 0$ can be obtained as the intersection of the four hypersurfaces $V = 0$, $E_B = 0$, $F_1 = 0$, $F_2 = 0$ with

$$F_1 = (c_2 - c_1)x_3 + (d_1 - d_2)y_3 + (c_1 - c_3)x_2, \quad F_2 = (d_2 - d_1)x_3 + (c_2 - c_1)y_3 + (d_1 - d_3)x_2, \quad (44)$$

where the latter two conditions are implied by Eq. (21).

Theorem 4. Singular points of the singularity variety $V_B = 0$ are also characterized by the four cases given in Theorem 3.

Proof. A singular point of $V_B = 0$ is either a singular point of one of the four hypersurfaces $V = 0$, $E_B = 0$, $F_1 = 0$, $F_2 = 0$ or it is a point, where the four tangent hyperplanes to these four hypersurfaces are linearly dependent. Algebraically this can be expressed by the set of equations resulting from the partial differentiation of

$$\lambda_0 V + \lambda_1 E_B + \lambda_2 F_1 + \lambda_3 F_2 \quad (45)$$

with respect to the 19 unknowns

$$c_1, \dots, c_6, d_1, \dots, d_6, x_2, x_3, y_3, \lambda_0, \dots, \lambda_3. \quad (46)$$

The corresponding result to Lemma 1 also holds with respect to $V_B = 0$, which is proven in Lemma 3 given in Appendix B. Therefore we can set $c_1 = d_1 = d_2 = 0$ in order to simplify the set of 19 equations, which allows us to solve them again by using Gröbner basis method implemented in `Maple`. The corresponding `Maple` file, which results in 48 solutions, can be downloaded from [16].

Out of the obtained 48 solutions, there are 24 solutions with $x_2 = 0$ contradicting our assumption $x_2 \neq 0$ implied by Lemma 2. There are 10 trivial solutions with $\lambda_0 = \lambda_1 = \lambda_2 = \lambda_3 = 0$. For the remaining 14 solutions $x_2 \neq 0$ holds true and $\lambda_1 = \lambda_2 = \lambda_3 = 0$. The latter already shows that these 14 solutions correspond to singular points of $V = 0$. \square

Clearly, this theorem also holds by exchanging the platform and the base which yields:

Theorem 5. *Singular points of the singularity variety $V_P = 0$ are also characterized by the four cases given in Theorem 3.*

If we restrict both base and platform to be transformed by Euclidean motions, then our set $V_{BP} = 0$ of singular configurations are obtained by intersecting the varieties $V_B = 0$ and $V_P = 0$. Note that the variety $V_P = 0$ is also obtained as the intersection of the four hypersurfaces $V = 0$, $E_P = 0$, $F_3 = 0$, $F_4 = 0$ with

$$F_3 = (c_5 - c_4)x_6 + (d_4 - d_5)y_6 + (c_4 - c_6)x_5, \quad F_4 = (d_5 - d_4)x_6 + (c_5 - c_4)y_6 + (d_4 - d_6)x_5 \quad (47)$$

where the latter two conditions are implied by Eq. (22).

Theorem 6. *Singular points of the singularity variety $V_{BP} = 0$ are also characterized by the four cases given in Theorem 3.*

Proof. A singular point of the singularity variety $V_{BP} = 0$ is either (I) a singular point of $V_B = 0$ or $V_P = 0$ or (II) it is a point, where the seven tangent hyperplanes to the seven hypersurfaces

$$V = 0, \quad E_B = 0, \quad E_P = 0, \quad F_1 = 0, \quad F_2 = 0, \quad F_3 = 0, \quad F_4 = 0, \quad (48)$$

are linearly dependent. Algebraically this can be expressed by the set of equations resulting from the partial differentiation of

$$\lambda_0 V + \lambda_1 E_B + \lambda_2 F_1 + \lambda_3 F_2 + \lambda_4 E_P + \lambda_5 F_3 + \lambda_6 F_4 \quad (49)$$

with respect to the 25 unknowns

$$c_1, \dots, c_6, d_1, \dots, d_6, x_2, x_3, x_5, x_6, y_3, y_6, \lambda_0, \dots, \lambda_6. \quad (50)$$

They form the following ideal:

$$\mathcal{I} := \langle g_1, \dots, g_{25} \rangle \subseteq \mathbb{K}[c_i, d_i, x_2, x_3, x_5, x_6, y_3, y_6, \lambda_0, \dots, \lambda_6] \quad i = 1, \dots, 6. \quad (51)$$

Similar to the procedure of Lemma 1 one can prove the translational invariance by substituting Eq. (40) into Eq. (51). We were not able to show the invariance under rotations by substituting Eq.

(42) into Eq. (51), as the ideal containment test failed due to the limited computational resources. Therefore we can set $c_1 = d_1 = 0$ but not $d_2 = 0$. Moreover, due to Lemma 2 given in Appendix B we can assume without loss of generality that $x_2x_5 \neq 0$ holds. Thus by assuming a suitable scale unit we can set $x_2x_5 = 1$. By adding this equation to the ideal of Eq. 51, we end up with:

$$\mathcal{I} := \langle g_1, \dots, g_{26} \rangle \subseteq \mathbb{K}[c_i, d_i, x_2, x_3, x_5, x_6, y_3, y_6, \lambda_0, \dots, \lambda_6] \quad i = 2, \dots, 6 \quad (52)$$

In the following, we prove that no singular points of type (II) exist. By setting $\lambda_j = 1$ for $j \in \{1, \dots, 6\}$ we obtain the ideal

$$\mathcal{I}_j := \langle g_1, \dots, g_{26} \rangle \subseteq \mathbb{K}[c_i, d_i, x_2, x_3, x_5, x_6, y_3, y_6, \lambda_0, \dots, \lambda_{j-1}, \lambda_{j+1}, \dots, \lambda_6] \quad i = 2, \dots, 6 \quad (53)$$

The corresponding basis with respect to graded reverse lexicographic order is denoted by \mathcal{B}_j . According to [18], *Hilbert's Nullstellensatz* implies that the variety of \mathcal{I}_j is empty if and only if $\mathcal{B}_j = \{1\}$. It can be verified by using `Maple` that $\mathcal{B}_j = \{1\}$ holds true. The used `Maple` file can be downloaded from [16].

Therefore the 25 equations g_i of Eq. (51), which are homogeneous with respect to $\lambda_0, \dots, \lambda_6$, can only have a solution for $(\lambda_0 : \lambda_1 : \dots : \lambda_6) = (1 : 0 : \dots : 0)$, but they belong to type (I). \square

4.1.1. Parametrizing the set of singular points of the singularity variety

In order to include the set of singular points of the singularity variety into our computation of the singularity distance we parameterize it. We restrict ourselves to the singular points, which correspond to case 1 of Theorem 3, as in practice no leg can have zero length thus cases 2-4 are not of interest. As case 1 of Theorem 3 is more restrictive than the collinearity conditions of Section 4.2 the following relations have to hold:

$$D_{\star}^{\blacktriangle}(\mathbf{K}, \mathbf{K}') \leq D_{\star}^{\blacktriangle}(\mathbf{K}, \mathbf{K}''), \quad D_{\Delta}^{\circ}(\mathbf{K}, \mathbf{K}') \leq D_{\Delta}^{\circ}(\mathbf{K}, \mathbf{K}'') \quad \text{with } \star, \circ \in \{\blacktriangle, \Delta, \blacksquare\} \quad (54)$$

where \mathbf{K}' is the global minimizer of Theorem 1 and 2, respectively, and \mathbf{K}'' denotes the closest singular point belonging to case 1 of Theorem 3.

Therefore one only has to compute \mathbf{K}'' for the metrics $D_{\star}^{\circ}(\mathbf{K}, \mathbf{K}'')$ with $\circ, \star \in \{\blacktriangle, \blacksquare\}$, which is done next:

- $D_{\blacktriangle}^{\blacktriangle}(\mathbf{K}, \mathbf{K}'')$: The point \mathbf{k}_1'' is parameterized by its coordinates $(a, b)^T$ and the remaining points by:

$$\mathbf{k}_{i+1}'' = \mathbf{k}_1'' + \delta_i \begin{pmatrix} e_0^2 - e_1^2 \\ 2e_0e_1 \end{pmatrix} \quad \text{for } i = 1, \dots, 5. \quad (55)$$

Now we minimize $D_{\blacktriangle}^{\blacktriangle}(\mathbf{K}, \mathbf{K}'')$ under the normalization condition $N = 0$ with $N := e_0^2 + e_1^2 - 1$, which results in the following Lagrangian formulation:

$$L = D_{\blacktriangle}^{\blacktriangle}(\mathbf{K}, \mathbf{K}'')^2 + \lambda N. \quad (56)$$

- $D_{\blacksquare}^{\blacktriangle}(\mathbf{K}, \mathbf{K}'')$: Clearly, \mathbf{K}'' can only exist if the base points of the given manipulator are collinear. If this is the case the parametrization can be done analogously to Eq. (55) with the sole difference that δ_1 and δ_2 are already known as they have to equal x_2 and x_3 , respectively.

Table 3: Summary of the Lagrange formulations of the optimization problems of Section 4.1.1.

Extrinsic metric	unknowns in the Lagrangian	# unknowns
$D_{\blacktriangle}^{\blacktriangle}(\mathbf{K}, \mathbf{K}')$	$a, b, \delta_1, \delta_2, \delta_3, \delta_4, \delta_5, e_0, e_1, \lambda$	10
$D_{\blacksquare}^{\blacktriangle}(\mathbf{K}, \mathbf{K}'), D_{\blacktriangle}^{\blacksquare}(\mathbf{K}, \mathbf{K}')$	$a, b, \delta_3, \delta_4, \delta_5, e_0, e_1, \lambda$	8
$D_{\blacksquare}^{\blacksquare}(\mathbf{K}, \mathbf{K}')$	$a, b, \delta_3, e_0, e_1, \lambda$	6

- $D_{\blacktriangle}^{\blacksquare}(\mathbf{K}, \mathbf{K}'')$: The same procedure can be applied as in the last case, just by swapping the roles of the platform and the base.
- $D_{\blacksquare}^{\blacksquare}(\mathbf{K}, \mathbf{K}'')$: Now \mathbf{K}'' can only exist if the given base points are collinear as well as the platform points. If this is the case the parametrization can be done as in Eq. (55) under consideration of $\delta_1 = x_2, \delta_2 = x_3$ with $\delta_4 = \delta_3 \pm x_5$ and $\delta_5 = \delta_3 \pm x_6$. Due to \pm one has to run two optimization problems with six unknowns $a, b, \delta_3, e_0, e_1, \lambda$ and take the minimum over both.

4.2. Singular points of the collinearity variety

It can easily be verified by the reader that the following theorem, which is illustrated in Fig. 7, holds true:

Theorem 7. *The singular points of the collinearity variety $C_B = 0$ (resp. $C_P = 0$) of the base (resp. platform) are characterized by $\mathbf{k}'_1 = \mathbf{k}'_2 = \mathbf{k}'_3$ (resp. $\mathbf{k}'_4 = \mathbf{k}'_5 = \mathbf{k}'_6$).*

As the condition that three points collapse to a single point is more restrictive than the condition that these three points are collinear the following relation has to hold:

$$D_{\star}^{\blacktriangle}(\mathbf{K}, \mathbf{K}') \leq D_{\star}^{\blacktriangle}(\mathbf{K}, \mathbf{K}'') \quad \text{for } \star \in \{\blacktriangle, \triangle\} \quad (57)$$

where \mathbf{K}' is the global minimizer of Theorem 1 and \mathbf{K}'' denotes the closest singular point of the collinearity variety $C_P = 0$. We only have to take a closer look at the case of equality in Eq. (57). According to the geometric interpretation given in Theorem 1 the three points $\mathbf{k}'_4, \mathbf{k}'_5, \mathbf{k}'_6$ can only collapse into one point if they are already collinear which contradicts our assumption that the given configuration is not singular. Therefore Eq. (57) can be sharpened as follows:

$$D_{\star}^{\blacktriangle}(\mathbf{K}, \mathbf{K}') < D_{\star}^{\blacktriangle}(\mathbf{K}, \mathbf{K}'') \quad \text{for } \star \in \{\blacktriangle, \triangle\}. \quad (58)$$

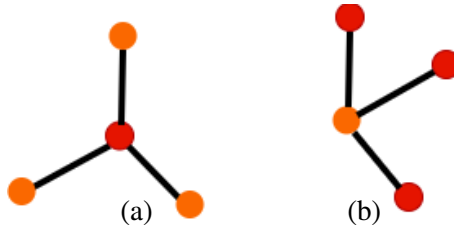


Figure 7: Schematic sketch of the geometric characterization of singular points of the collinearity variety (a) $C_P = 0$ (b) $C_B = 0$. Base and platform anchor points are indicated in orange and red, respectively.

Analogous considerations to the above case yield the inequality

$$D_{\Delta}^{\circ}(\mathbf{K}, \mathbf{K}') < D_{\Delta}^{\circ}(\mathbf{K}, \mathbf{K}'') \quad \text{for } \circ \in \{\blacktriangle, \triangle\}, \quad (59)$$

where \mathbf{K}' is the global minimizer of Theorem 2 and \mathbf{K}'' denotes the closest singular point of the collinearity variety $C_B = 0$.

Due to the validity of the Eqs. (58) and (59), we can abstain from computing the configurations \mathbf{K}'' for the respective metrics.

If we restrict the base (resp. platform) to be transformed by Euclidean motions, then our set of collinear configurations is only a subset \tilde{C}_P (resp. \tilde{C}_B) of C_P (resp. C_B). The singular points of these subsets have the same geometric characterization as given in Theorem 7, which is proven next:

Theorem 8. *Singular points of the collinearity variety $\tilde{C}_P = 0$ are characterized by $\mathbf{k}'_4 = \mathbf{k}'_5 = \mathbf{k}'_6$.*

Proof. A singular point of $\tilde{C}_P = 0$ is either a singular point of one of the four hypersurfaces $C_P = 0$, $E_B = 0$, $F_1 = 0$, $F_2 = 0$ or it is a point, where the four tangent hyperplanes to these four hypersurfaces are linearly dependent. Algebraically this can be expressed by the set of equations resulting from the partial differentiation of

$$\lambda_0 C_P + \lambda_1 E_B + \lambda_2 F_1 + \lambda_3 F_2 \quad (60)$$

with respect to the 19 unknowns listed in Eq. (46). This square system of equations is solved by using Gröbner basis method implemented in `Maple`. The corresponding `Maple` file, which results in 36 solutions, can be downloaded from [16].

Out of the obtained 36 solutions, there are 34 solutions with $x_2 = 0$, which contradicts with Lemma 2. Moreover there is one trivial solution with $\lambda_0 = \lambda_1 = \lambda_2 = \lambda_3 = 0$ (and $x_2 \neq 0$). The remaining solution corresponds to the singular point of $C_P = 0$. \square

Clearly, this theorem also holds by exchanging the platform and the base which yields:

Theorem 9. *Singular points of the collinearity variety $\tilde{C}_B = 0$ are characterized by $\mathbf{k}'_1 = \mathbf{k}'_2 = \mathbf{k}'_3$.*

If the base or platform is made of undeformable material we have to compute the closest singular points \mathbf{K}'' , on the collinearity varieties $\tilde{C}_P = 0$ and $\tilde{C}_B = 0$ of Theorems 8 and 9, which can be done by solving the optimization problems formulated in the following two equations:

$$L = D_{\blacksquare}^{\Delta}(\mathbf{K}, \mathbf{K}'')^2 + \mu E_B, \quad (61)$$

where the three platform anchor points of \mathbf{K}'' degenerate to a point $\mathbf{k}'' := (c, d)^T$ and with \mathbf{k}''_3 according to Eq. 21;

$$L = D_{\Delta}^{\blacksquare}(\mathbf{K}, \mathbf{K}'')^2 + \kappa E_P, \quad (62)$$

where the three base anchor points of \mathbf{K}'' degenerate to a point $\mathbf{k}'' := (c, d)^T$ and with \mathbf{k}''_6 according to Eq. 22. The number of unknowns for these two optimization problems is summarized in Table 4.

Table 4: Summary of the Lagrange formulations of the constrained optimization problems of Section 4.2.

Extrinsic metric	unknowns in the Lagrangian	# unknowns
$D_{\Delta}^{\wedge}(\mathbf{K}, \mathbf{K}')$	$c_1, d_1, c_2, d_2, c, d, \mu$	7
$D_{\Delta}^{\square}(\mathbf{K}, \mathbf{K}')$	$c, d, c_4, d_4, c_5, d_5, \kappa$	7

5. Computational procedure

In this section, we present a pipeline for computing the closest singular configuration along a one-parametric motion, which is discretized into n poses, for the presented nine interpretations illustrated in Fig. 3. We use numerical algebraic geometry algorithms implemented in the freeware `Bertini` for computing generic finite solutions and for user-defined homotopy. We compute critical points for each of the n poses along the one parametric motion by using `Paramotopy` [11]. The practical reasons for using the software `Bertini` are discussed in [15, Section 1]. A detailed discussion of homotopy continuation algorithms and the functioning of the software is not within the scope of the paper, for that we refer to [9, 19].

The computations were performed in parallel using a total of 64 threads using AMD Ryzen 7 2700X, 3.7 GHz processor. The computational procedure can be divided into four steps, which are discussed within the following subsections and are illustrated in Fig. 8 of the operational flowchart.

5.1. Step 1: Ab-Initio phase

We start with a generic framework by picking randomly all nine remaining coordinates (besides $c_1 = d_1 = d_2 = 0$) with respect to the fixed frame from the set of complex numbers \mathbb{C} . Therefore, we denote the resulting vectors of the anchor points with respect to the fixed frame by $\mathbf{k}_i^{\mathbb{C}}$ for $i = 1, \dots, 6$ and consequently the complex configuration by $\mathbf{K}^{\mathbb{C}}$, which is called *source configuration*. For this input, we want to find the critical points over \mathbb{C} , for each of the Lagrange optimization problems formulated in Section 3.1, Section 3.2, and Section 4.1.1 and Section 4.2. The corresponding unknowns in L for the optimization problems are summarized in Table 1, Table 3, and Table 4, respectively. As already mentioned the number of unknowns for the optimization problems presented in Section 3.2 is the same as summarized in Table 1.

Note that the partial derivatives of L with the listed unknowns always result in the square system of non-homogeneous polynomial equations. The critical points obtained from the *ab-initio phase* are referred to as solutions to the *source configuration*.

As `Bertini` computes solutions to the system of polynomial equations with numerical approximations up to 16 digits (default), it is not possible to know the exact root count beforehand, without tracking all the paths. For the optimization problems presented in Section 3.1, Section 3.2 Section 4.1.1 and Section 4.2, we have to find the global minimizers as they correspond to the closest singular configuration. Therefore it is necessary to track all the finite solutions over \mathbb{C} without any numerical errors (e.g. path failures) in the ab-initio phase.

The input file required for `Bertini` to compute the solutions of the source configuration is pre-processed in `Maple`. It has to be noted that the `Bertini` package allows numerous configuration settings in the input file to track solutions without path failures. Currently, there is no artificial intelligence module implemented in `Bertini1.6v` in order to indicate the necessary

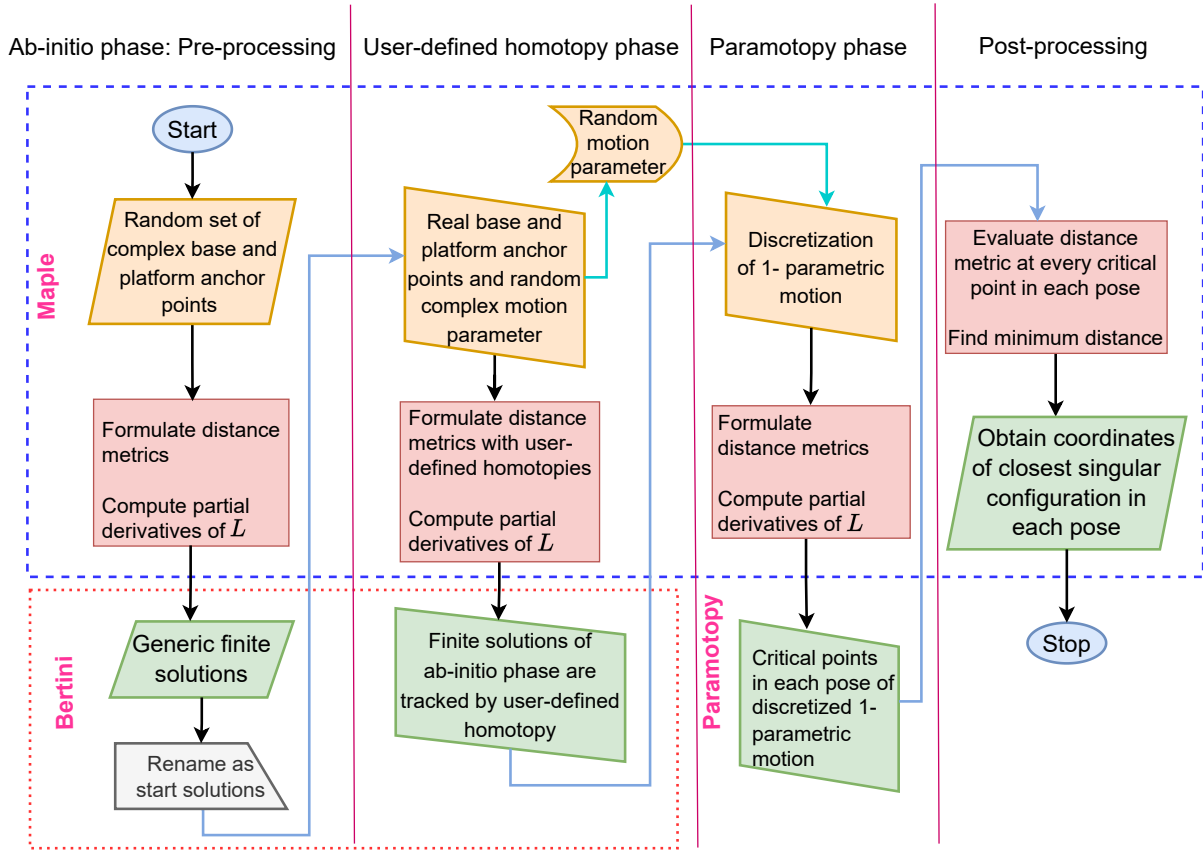


Figure 8: Operational flowchart of the computational pipeline.

configuration settings required for the given input file given by the user, to track the solutions without numerical errors. Therefore, they have to be fine-tuned manually to the problem at hand. We refer to [10, p. 301-321] for understanding configuration settings in detail.

First of all, we have to check if the solution sets of the presented optimization problems contain any higher dimensional components. This can be done in `Bertini` by invoking `Tracktype:1` in the configuration settings of the input files by keeping the remaining settings as default. It shows that no higher dimensional components exist for the source configuration. Thus we can proceed with the computation of the isolated solutions using the regeneration algorithm [20] implemented in `Bertini1.6v5`, which finds the solution to the systems by sequentially solving equation-by-equation but has the following limitation.

Limitation 1. According to [10, p. 93] using the regeneration algorithm, it is not guaranteed to obtain all the solutions as it discards singular solutions during the computation.

As already mentioned we need to obtain all the generic finite solutions (including singular solutions). By using symbolic methods (e.g. Gröbner basis method within `Maple`), we are able to

⁵Note that in `HC.jl` regeneration algorithm is not implemented.

reduce each optimization problem to the solution of a univariate polynomial. Its degree corresponds to the root count, which can be used to check if all solutions were tracked by the regeneration algorithm performed with the configuration settings given in Table 5. This is the case according to Tables 6–9. Note that these generic solutions only have to be computed once for each of the different optimization problems.

Table 5: Configuration settings used for the regeneration algorithm in the ab-initio phase.

Configuration settings	value	Configuration settings	value
TRACKToIBeforeEG	1e-8	TRACKToIDURINGEG	1e-8
SliceToIBeforeEG	1e-8	SliceToIDuringEG	1e-8
SECURITYLEVEL	1	UseRegeneration	1

Table 6: Summary of generic finite solutions from the ab-initio phase for the Lagrangians formulated in Section 3.1.

Extrinsic metric	# finite solutions over \mathbb{C} (Bertini)	degree of univariate polynomial (Maple)
$D_{\square}^{\square}(\mathbf{K}, \mathbf{K}')$	88	88
$D^{\circ}(\mathbf{K}, \mathbf{K}')$ with $\circ \in \{\blacktriangle, \triangle\}$	80	80
$D_{\star}^{\square}(\mathbf{K}, \mathbf{K}')$ with $\star \in \{\blacktriangle, \triangle\}$	80	80
$D_{\star}^{\circ}(\mathbf{K}, \mathbf{K}')$ with $\circ, \star \in \{\blacktriangle, \triangle\}$	50	50

Table 7: Summary of generic finite solutions from the ab-initio phase for the Lagrangians formulated in Section 3.2

Extrinsic metric	# finite solutions over \mathbb{C} (Bertini)	degree of univariate polynomial (Maple)
$D_{\square}^{\blacktriangle}(\mathbf{K}, \mathbf{K}'), D_{\triangle}^{\square}(\mathbf{K}, \mathbf{K}')$	8	8
$D_{\star}^{\blacktriangle}(\mathbf{K}, \mathbf{K}'), D_{\triangle}^{\circ}(\mathbf{K}, \mathbf{K}')$ with $\star, \circ \in \{\blacktriangle, \triangle\}$	2	2

Table 8: Summary of generic finite solutions from the ab-initio phase for the Lagrangians formulated in Section 4.1.1

Extrinsic metric	# finite solutions over \mathbb{C} (Bertini)	degree of univariate polynomial (Maple)
$D_{\square}^{\square}(\mathbf{K}, \mathbf{K}')$	8	8
$D_{\square}^{\blacktriangle}(\mathbf{K}, \mathbf{K}'), D_{\blacktriangle}^{\square}(\mathbf{K}, \mathbf{K}')$	8	8
$D_{\blacktriangle}^{\blacktriangle}(\mathbf{K}, \mathbf{K}')$	8	8

5.2. Step 2: User-defined homotopy phase

The input for this step is the geometry of the manipulator given by the real values $x_2, x_3, y_3, x_5, x_6, y_6$ and a 1-parametric motion with parameter $\phi \in [v; w]$; i.e.

$$\mathbf{k}_j(\phi) = \mathbf{R}(\phi)\mathbf{p}_j + \mathbf{t}(\phi) \quad \text{for } j = 4, 5, 6 \quad (63)$$

Table 9: Summary of generic finite solutions from the ab-initio phase for the Lagrangians formulated in Section 4.2

Extrinsic metric	# finite solutions over \mathbb{C} (Bertini)	degree of univariate polynomial (Maple)
$D_{\square}^{\Delta}(\mathbf{K}, \mathbf{K}'), D_{\Delta}^{\square}(\mathbf{K}, \mathbf{K}')$	2	2

according to Eq. (1). We consider one generic random complex pose of this motion, referred to as *seed configuration*, by setting

$$\phi^{\mathbb{C}} = v - (v - w)(1 - \alpha^{\mathbb{C}}) \quad (64)$$

where $\alpha^{\mathbb{C}}$ is a randomly chosen complex number. Now we define a linear homotopy between the vector coordinates of the ab-initio configuration $\mathbf{k}_i^{\mathbb{C}}$ and the seed configuration by

$$\begin{aligned} \mathbf{k}_i^{\mathbb{C}} &\mapsto \mathbf{k}_i + m(\mathbf{k}_i^{\mathbb{C}} - \mathbf{k}_i) & \text{for } j = 1, 2, 3 \\ \mathbf{k}_i^{\mathbb{C}} &\mapsto \mathbf{k}_i(\phi^{\mathbb{C}}) + m(\mathbf{k}_i^{\mathbb{C}} - \mathbf{k}_i(\phi^{\mathbb{C}})) & \text{for } j = 4, 5, 6 \end{aligned} \quad (65)$$

where m is the homotopy parameter. By applying this mapping to the polynomial systems of the ab-initio phase, we are able to track the finite solutions of the *source configuration* to the finite solutions of the *seed configuration* while m is running from 1 to 0.

5.3. Step 3: Paramotopy phase

The usage of Paramotopy [11] software comes with two steps. Based on an input file, Paramotopy calls in a first step Bertini to solve the system of polynomial equations at a generic parameter point. These solutions are tracked by Paramotopy in a second step to all desired parameter values again by calling Bertini.

With our *seed configuration* and its solutions computed in Section 5.2 we can directly enter the second step of Paramotopy, which requires in addition the parameter $\alpha^{\mathbb{C}}$ and the number n of poses (can be defined by the user), in which the 1-parametric motion of Eq. (63), should be discretized. In fact, $\alpha \in [0; 1]$ is equally subdivided into n values, and while α runs through this interval the corresponding solutions for the n poses are tracked by Paramotopy. While running Step 2 of paramotopy there can still be path failures for each discretized pose, to overcome these failures one needs to re-run failed paths by tuning the configuration settings.

5.4. Step 4: Post-processing

In this phase, the obtained real solutions for n discretized poses are given as input to Maple. For the corresponding configuration, the distance function is evaluated in order to filter out the global minimizer.

5.5. Interface

To operate this pipeline, we developed an open-source software interface between Maple and Bertini as well as Paramotopy, thus that all calls can be made within Maple rather than by switching between the systems. Note that the user needs to run only steps 2–4.

Remark 3. Steps 2 and 3 of the above given computational pipeline can also be replaced by using both steps of *Paramotopy* [11]. The drawback is that one always needs to run the first step of *Paramotopy* which is substantially longer, as it can be seen from Table 10, which lists the computation times for the numerical example discussed in the next section. \diamond

6. Results and discussion

The presented computational procedure for finding singularity distances is demonstrated on the basis of the following numerical example for all the optimization problems. The base and platform anchor points and the one parametric motion are given by:

$$\mathbf{k}_1 = \mathbf{p}_1 = (0, 0), \quad \mathbf{k}_2 = (11, 0), \quad \mathbf{p}_2 = (3, 0), \quad \mathbf{k}_3 = (5, 7), \quad \mathbf{p}_3 = (1, 2) \quad (66)$$

and

$$\mathbf{k}_{i+3} = \underbrace{\begin{pmatrix} \cos \phi & -\sin \phi \\ \sin \phi & \cos \phi \end{pmatrix}}_{\mathbf{R}} \mathbf{p}_i + \frac{1}{2} \underbrace{\begin{pmatrix} 11 - 6 \sin \phi \\ 3 - 3 \cos \phi \end{pmatrix}}_{\mathbf{t}} \quad \text{for } i = 1, 2, 3. \quad (67)$$

Note that this 1-parametric motion of the manipulator has two singular configurations at $\phi = 0$ and $\phi \approx 3.0356972$ radians. The interval for the motion parameter ϕ is chosen between $[0; 2\pi]$; i.e. $v = 0$ and $w = 2\pi$. According to Eq. (64) we generate a floating point arithmetic of a random complex α^c and express the pose of the platform with respect to the base frame by Eq. (67). By defining user-defined homotopies given by Eq. (65), we obtain the system of polynomial equations depending on the homotopy parameter m . We invoke `User homotopy: 2` in the input files, to avoid tracking infinitely long paths (for details see [10, Sec. 7.5.2]). We use generic finite solutions of the *source configuration* as `start solutions` and track them to the *seed configuration* without any path failures. Note that the number of paths to be tracked equals the generic finite root count given in Tables 6–9. For the *Paramotopy* phase we set $n = 90$; i.e. we discretized the 1-parametric motion into 90 poses. The resulting solution set for each pose is post-processed according to Step 4. A comparison of the average CPU run time⁶ (over 5 runs) between both steps of *Paramotopy* and Step 2 and Step 3 of the proposed algorithm is given in Table 10.

In Fig. 9 we compare the distances to the singularity variety $V = 0$ with respect to the different extrinsic metrics $D_{\star}^{\circ}(\mathbf{K}, \mathbf{K}')$ with $\circ, \star \in \{\blacktriangle, \triangle, \blacksquare\}$ to the preliminary one $D_{\star}^{\bullet}(\mathbf{K}, \mathbf{K}')$ of Eq. (3). Note that due to the discretization of the motion into 90 poses by *Paramotopy*, the linearly interpolated value at the singularity $\phi \approx 3.0356972$ radians is not exactly zero. In Fig. 10 the closest singular configurations on $V = 0$ are illustrated for the pose $\phi = 0.8471710528$, which is indicated by the black dashed line in Fig. 9. For the metric $D_{\star}^{\bullet}(\mathbf{K}, \mathbf{K}')$ we refer to Fig. 2.

For the interpretations possessing a pin-jointed triangular bar structure in the platform or base, the distances to the singularity variety and collinearity variety are compared in Fig. 11. In Fig. 12 the corresponding closest configurations on the collinearity varieties are again illustrated for the pose $\phi = 0.8471710528$.

⁶In this context we are referring to *response time*.

Table 10: A comparison of average run time (in seconds) for Step 2 and Step 3 and both steps of Paramotopy.

Extrinsic metric	A) Step 2	B) Step 3	C) both steps of Paramotopy	Ratio $C/(A + B)$
$D_{\square}^{\square}(\mathbf{K}, \mathbf{K}')$	≈ 2.160	≈ 236.861	≈ 651.200	≈ 2.152
$D_{\square}^{\Delta}(\mathbf{K}, \mathbf{K}')$	≈ 4.074	≈ 263.130	$\approx 5\,100.240$	≈ 19.087
$D_{\Delta}^{\square}(\mathbf{K}, \mathbf{K}')$	≈ 2.860	≈ 292.250	$\approx 5\,563.370$	≈ 18.851
$D_{\Delta}^{\Delta}(\mathbf{K}, \mathbf{K}')$	≈ 4.258	≈ 315.413	$\approx 5\,152.523$	≈ 17.244
$D_{\Delta}^{\square}(\mathbf{K}, \mathbf{K}')$	≈ 1.640	≈ 104.636	$\approx 6\,595.126$	≈ 62.056
$D_{\Delta}^{\Delta}(\mathbf{K}, \mathbf{K}')$	≈ 1.056	≈ 160.260	$\approx 5\,915.350$	≈ 36.669
$D_{\Delta}^{\square}(\mathbf{K}, \mathbf{K}')$	≈ 3.686	≈ 276.653	$\approx 5\,548.023$	≈ 19.790
$D_{\Delta}^{\Delta}(\mathbf{K}, \mathbf{K}')$	≈ 1.280	≈ 147.720	$\approx 6\,063.070$	≈ 40.691
$D_{\Delta}^{\Delta}(\mathbf{K}, \mathbf{K}')$	≈ 1.778	≈ 113.292	$\approx 6\,731.132$	≈ 58.495

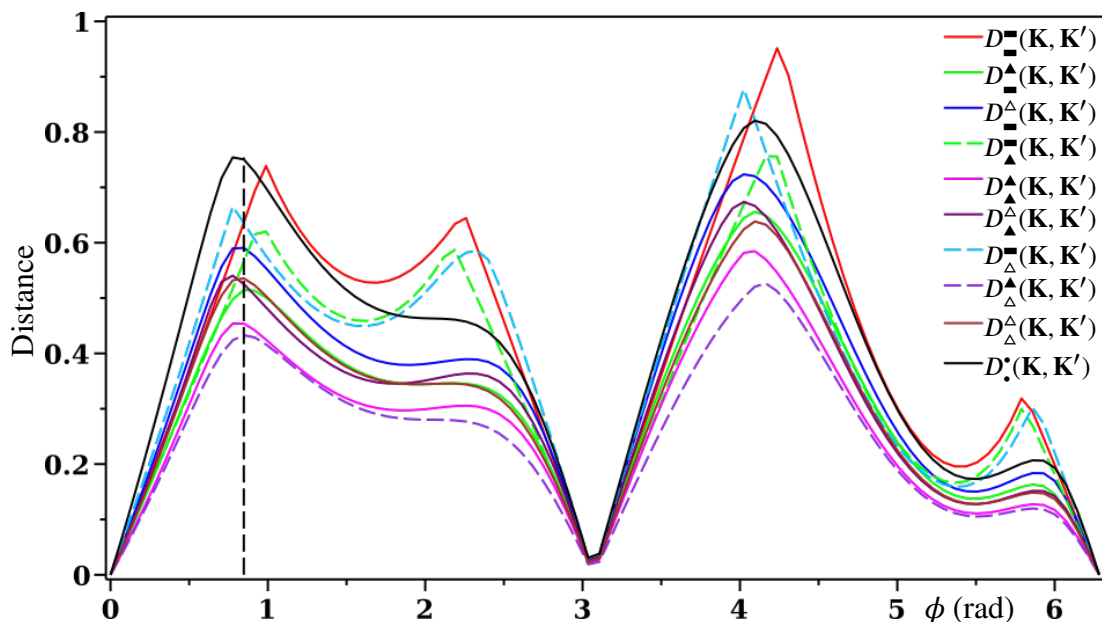


Figure 9: Distances to the singularity variety $V = 0$ with respect to the different extrinsic metrics.

In Fig. 13 (a,b,c), we present the comparison of the distances to the closest regular and singular points of the constraint variety. It can be observed that the latter is always larger. The configuration, which corresponds to the closest singular point on the constraint variety, is illustrated in Fig. 13 (d,e,f) for the pose $\phi = 0.8471710528$.

Remark 4. *The animations of the manipulator's one-parametric motion given in Eq. 67 together with the closest singular configurations implying the graphs of Figs. 9, 11 and 13 can be downloaded from [16].* \diamond

For the singularity distance, we have to take the minimum of the graphs given in Figs. 9, 11 and 13, which yields the graphs given in Fig. 14. Finally, we want to point out that discontinuities in the final graphs of Fig. 14 belong to the cut loci of the extrinsic distance functions; i.e. in the

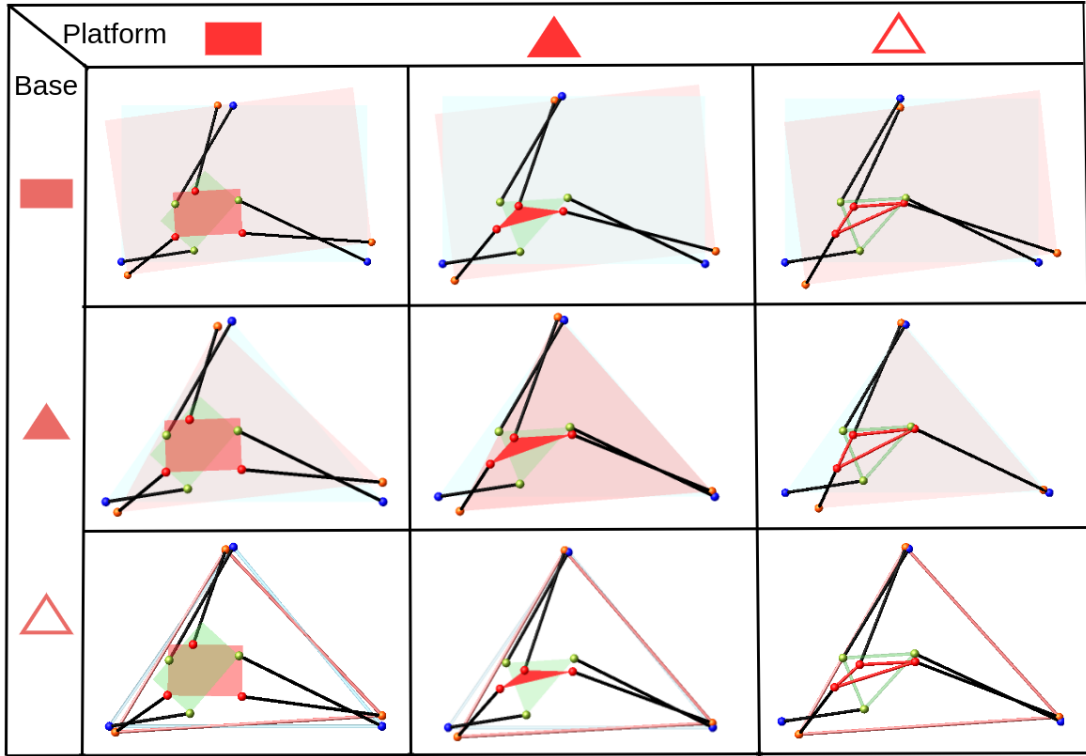


Figure 10: Closest singular configurations on $V = 0$ for $\phi = 0.8471710528$ radians.

corresponding configurations the closest singular configuration is not determined uniquely (there exist at least two closest singular configurations).

7. Conclusion and future work

We presented extrinsic metrics for the computation of the closest singular configuration of a 3-RPR parallel manipulator, which takes the combinatorial structure of the mechanism into account as well as different design options. For each of the resulting nine interpretations (Section 1.3) the corresponding extrinsic metric relies on the distance computation between structural components (Section 2).

The constrained optimization problem of computing the closest singular configuration with respect to these nine metrics was formulated using the Lagrangian approach (Section 3). As the singular points of the constraint varieties are missed by this method, we determined them algebraically. Based on their obtained geometric characterization, we parameterized them for a separate optimization (Section 4).

Moreover, we presented an efficient computational algorithm for the singularity distance computation along a 1-parametric motion of the manipulator using the computer algebra system `Maple` as well as the numerical algebraic geometry software `Bertini` and `Paramotopy` (Section 5). We coded an open-source software interface allowing to make all calls from `Maple` rather than by

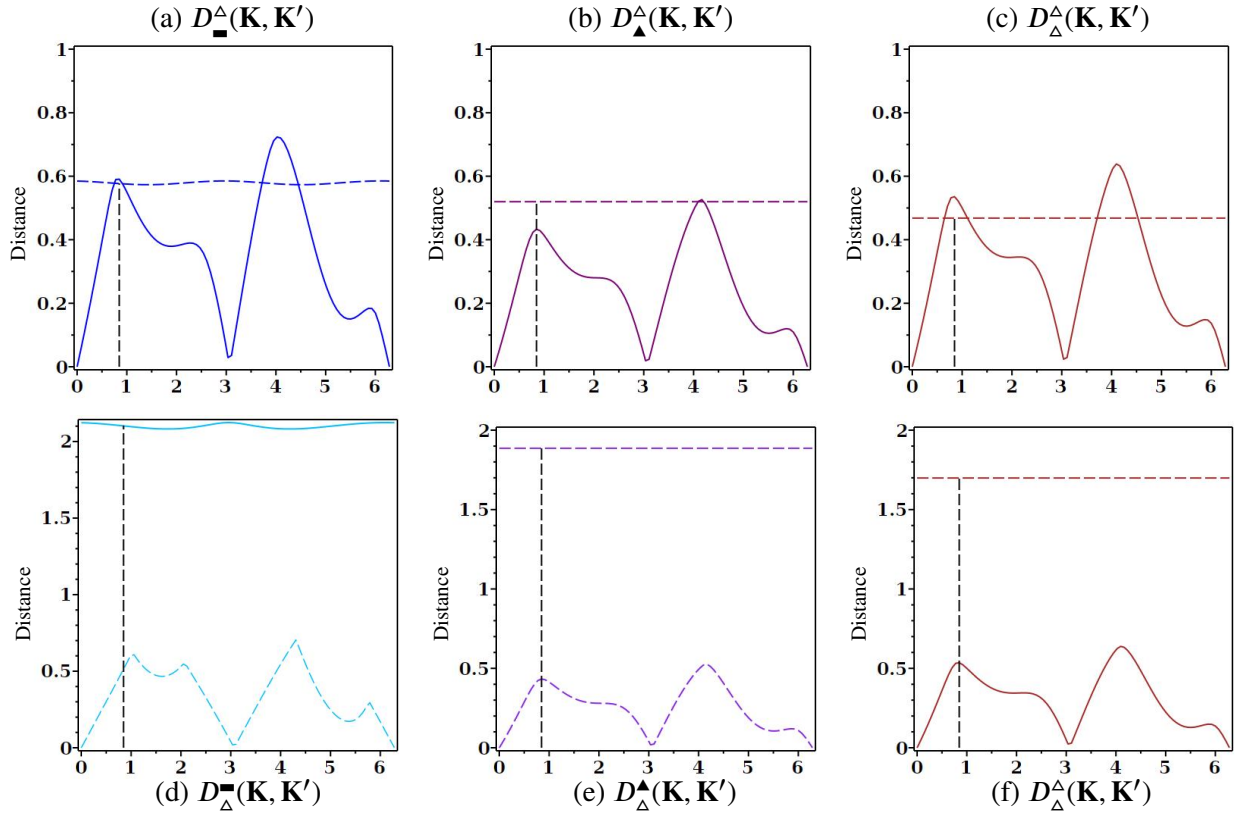


Figure 11: Comparison of distances to the singularity variety $V = 0$ and the collinearity variety $C_P = 0$ (top) and $C_B = 0$ (bottom), respectively.

switching between the systems. Finally, we validated our approach on hand of a numerical example (Section 6).

Due to the possibility of parallelizing the computations, the proposed singularity distance algorithm has the capability to be executed in real-time, which can be used for singularity-free path planning. In [3], we studied for the same nine interpretations of 3-RPR configurations the computation of singularity distances with respect to intrinsic metrics and compared them to the corresponding extrinsic ones. As already mentioned in Remark 1, the paired intrinsic and extrinsic metrics can be used for sensitivity analysis, which is dedicated to future research.

Finally it should be noted, that the presented method of computing the extrinsic distance to the closest singularity can adopted straightforwardly to any robot, which can be abstracted into a jointed composition of bars, triangular plates and tetrahedral bodies. For the latter ones a similar formula to Eq. (7) can be computed in analogy to Appendix A.

Acknowledgement

This research is supported by Grant No. P 30855-N32 of the Austrian Science Fund FWF. The first author would like to thank Silvana Amethyst for valuable suggestions and technical talks on Bertini/Paramotopy.

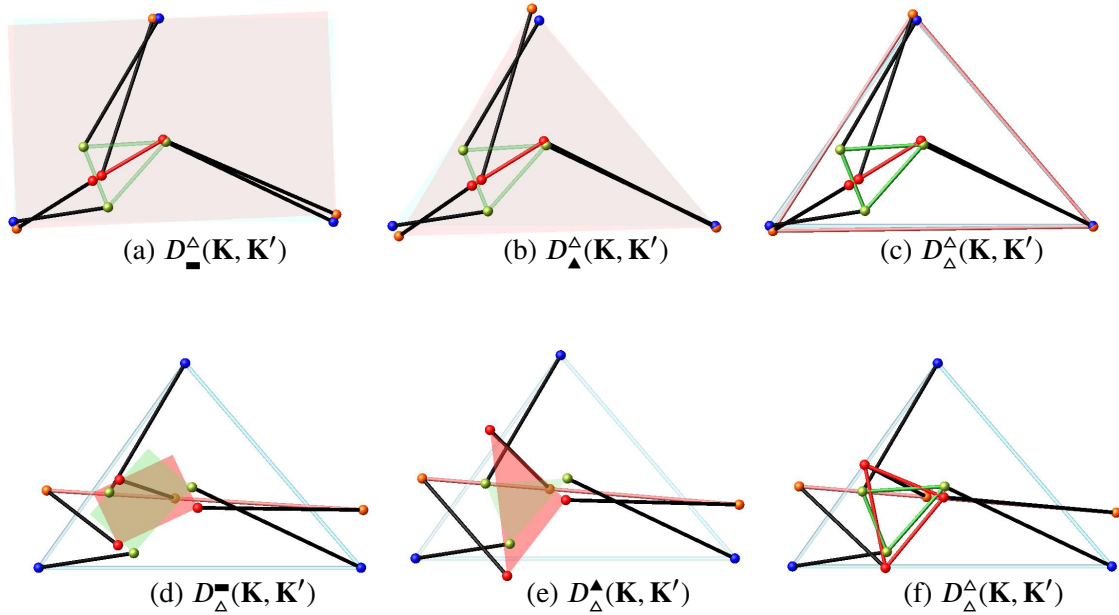


Figure 12: Closest singular configurations on the collinearity variety $C_P = 0$ (top) and $C_B = 0$ (bottom), respectively, for $\phi = 0.8471710528$ radians.

References

- [1] J. Merlet, *Parallel Robots*, Vol. 128, Springer Science & Business Media, 2006.
- [2] J.-P. M. J. Hubert, Static of parallel manipulators and closeness to singularity, *Journal of Mechanisms Robotics* 1 (1) (2008) 1–6.
- [3] A. Kapilavai, G. Nawratil, Singularity distance computations for 3-RPR manipulators using intrinsic metrics, in preparation.
- [4] A. Rasoulzadeh, G. Nawratil, Variational path optimization of linear pentapods with a simple singularity variety, *Mechanism and Machine Theory* 153 (2020) 104002.
- [5] J. Angeles, *Theory, Methods, and Algorithms*, 2nd Edition, Springer-Verlag New York, 2002.
- [6] H. Li, C. M. Gosselin, M. J. Richard, Determination of maximal singularity-free zones in the workspace of planar three-degree-of-freedom parallel mechanisms, *Mechanism and Machine Theory* 41 (10) (2006) 1157–1167.
- [7] G. Abbasnejad, H. M. Daniali, S. M. Kazemi, A new approach to determine the maximal singularity-free zone of 3-RPR planar parallel manipulator, *Robotica* 30 (6) (2012) 1005–1012.
- [8] G. Nawratil, Singularity distance for parallel manipulators of Stewart Gough type, in: T. Uhl (Ed.), *Advances in Mechanism and Machine Science*, Springer, 2019, pp. 259–268.
- [9] D. J. Bates, J. D. Hauenstein, A. J. Sommese, C. W. Wampler, *Bertini: Software for numerical algebraic geometry*, Available at bertini.nd.edu with permanent doi: [dx.doi.org/10.7274/R0H41PB5](https://doi.org/10.7274/R0H41PB5) (2013).
- [10] D. J. Bates, A. J. Sommese, J. D. Hauenstein, C. W. Wampler, *Numerically solving polynomial systems with Bertini*, SIAM, 2013.
- [11] D. Bates, D. Brake, M. Niemerg, Paramotopy: Parameter homotopies in parallel, in: *International Congress on Mathematical Software*, Springer, 2018, pp. 28–35.
- [12] S. Caro, N. Binaud, P. Wenger, Sensitivity analysis of 3-RPR planar parallel manipulators, *Journal of mechanical design* 131 (12).

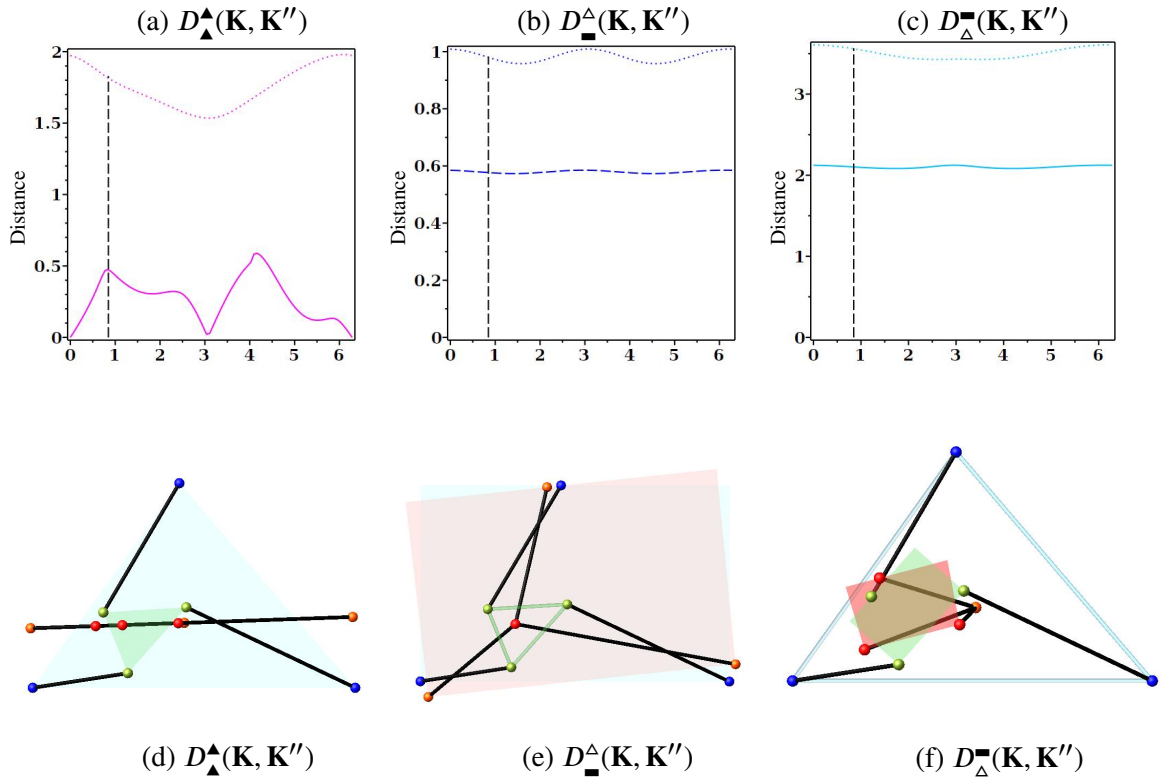


Figure 13: Comparison of the distances to the closest regular and singular points of the constraint variety, (a) $V = 0$, (b) $C_P = 0$, and (c) $C_B = 0$, respectively. The configuration, which corresponds to the closest singular point on the constraint variety (a,b,c), is illustrated in (d,e,f) for $\phi = 0.8471710528$ radians.

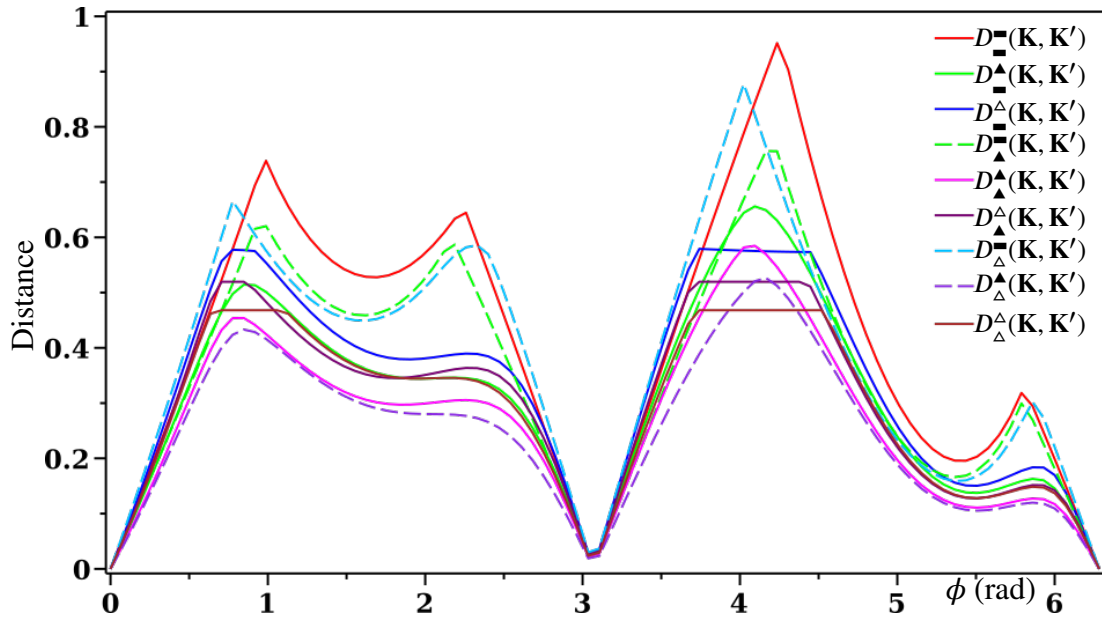


Figure 14: Singularity distances with respect to the presented extrinsic metrics.

- [13] H.-Y. Chen, H. Pottmann, Approximation by ruled surfaces, *Journal of computational and Applied Mathematics* 102 (1) (1999) 143–156.
- [14] G. Nawratil, Point-models for the set of oriented line-elements – a survey, *Mechanism and Machine Theory* 111 (2017) 118–134.
- [15] A. Kapilavai, G. Nawratil, On homotopy continuation based singularity distance computations for 3-RPR manipulators, in: *European Conference on Mechanism Science*, Springer, 2020, pp. 56–64.
- [16] Git repository, <https://github.com/aditya-kapilavai>, accessed: 2023-04-02 (2023).
- [17] M. Husty, On singularities of planar 3-RPR parallel manipulators, in: *Proceedings of the 14th IFToMM World Congress*, Vol. 4, IFToMM, 2015, pp. 2325–2330.
- [18] B. Sturmfels, What is... a grobner basis?, *Notices-American Mathematical Society* 52 (10) (2005) 1199.
- [19] A. J. Sommese, C. W. Wampler, et al., *The Numerical solution of systems of polynomials arising in engineering and science*, World Scientific, 2005.
- [20] J. Hauenstein, A. Sommese, C. Wampler, Regeneration homotopies for solving systems of polynomials, *Mathematics of Computation* 80 (273) (2011) 345–377.

Appendix A. Derivation of the distance between triangular plates

The triangular plate \blacktriangle_{ijk} in \mathbb{R}^2 can be captured by the affine combinations of its vertices $\mathbf{k}_i, \mathbf{k}_j, \mathbf{k}_k$; i.e.

$$\blacktriangle_{ijk} : u \mathbf{k}_i + v \mathbf{k}_j + (1 - u - v) \mathbf{k}_k \quad \text{with } u \in [0, 1], v \in [0, 1 - u]. \quad (\text{A.1})$$

In order to define a distance function between two triangles $\blacktriangle_{ijk} = (\mathbf{k}_i, \mathbf{k}_j, \mathbf{k}_k)$ and $\blacktriangle'_{ijk} = (\mathbf{k}'_i, \mathbf{k}'_j, \mathbf{k}'_k)$ illustrated in Fig. 4 we use the parameterization of Eq. (A.1) to view both triangles as images of the unit triangle T_0 under the following two affine mappings:

$$\psi_{\blacktriangle_{ijk}} : \begin{pmatrix} u \\ v \end{pmatrix} \mapsto u \mathbf{k}_i + v \mathbf{k}_j + (1 - u - v) \mathbf{k}_k \quad \text{with } u \in [0, 1], v \in [0, 1 - u], \quad (\text{A.2})$$

$$\psi_{\blacktriangle'_{ijk}} : \begin{pmatrix} u \\ v \end{pmatrix} \mapsto u \mathbf{k}'_i + v \mathbf{k}'_j + (1 - u - v) \mathbf{k}'_k \quad \text{with } u \in [0, 1], v \in [0, 1 - u]. \quad (\text{A.3})$$

Now we define the distance as the integral over the pointwise distances of corresponding triangle points by:

$$\begin{aligned} & \frac{1}{|T_0|} \int_{T_0} \left(\psi_{\blacktriangle_{ijk}} - \psi_{\blacktriangle'_{ijk}} \right)^2 dA = \\ & 2 \int_0^1 \int_0^{1-u} \left[u (\mathbf{k}_i - \mathbf{k}'_i) + v (\mathbf{k}_j - \mathbf{k}'_j) + (1 - u - v) (\mathbf{k}_k - \mathbf{k}'_k) \right]^2 du dv \end{aligned} \quad (\text{A.4})$$

where A denotes the area. By solving Eq. (A.4) we obtain the squared distance between two triangles \blacktriangle_{ijk} and \blacktriangle'_{ijk} given in Eq. (7).

Appendix B. Lemmata

Lemma 2. *For a 3-RPR manipulator, which is not architecturally singular, there always exists pairwise distinct indices $i, j \in \{1, 2, 3\}$ such that $\mathbf{k}_i \neq \mathbf{k}_j$ and $\mathbf{k}_{i+3} \neq \mathbf{k}_{j+3}$ hold true.*

Proof. From the geometric point of view, a 3-RPR manipulator is only architecturally singular if and only if either the base or platform collapses to a point.

Suppose that $\mathbf{k}_1, \mathbf{k}_2, \mathbf{k}_3$ are pairwise distinct. As the manipulator is not architectural singular, there has to exist a pair of indices $i, j \in \{1, 2, 3\}$ such that $\mathbf{k}_{i+1} \neq \mathbf{k}_{j+1}$ holds, and we are done.

Suppose now that a pair of points among $\mathbf{k}_1, \mathbf{k}_2, \mathbf{k}_3$ coincide; without loss of generality we can assume $\mathbf{k}_1 = \mathbf{k}_2$. As the manipulator is not architecturally singular, \mathbf{k}_3 is distinct from $\mathbf{k}_1 = \mathbf{k}_2$. Now either $\mathbf{k}_4 \neq \mathbf{k}_6$ has to hold or $\mathbf{k}_5 \neq \mathbf{k}_6$, as otherwise this would imply the architecture singularity $\mathbf{k}_4 = \mathbf{k}_5 = \mathbf{k}_6$. \square

Lemma 3. *The set of singular points of the singularity variety $V_B = 0$ remains invariant under Euclidean motions.*

Proof. From Eq. (45) it can be seen that V_B depends on the free coordinates c_i, d_i ($i = 1, \dots, 6$), the base design parameters x_2, x_3, y_3 and the multipliers $\lambda_0, \dots, \lambda_3$. Partial derivatives of Eq. (45) with respect to these 19 unknowns form the following ideal:

$$\mathcal{I} := \langle g_1, \dots, g_{19} \rangle \subseteq \mathbb{K}[c_i, d_i, x_2, x_3, y_3, \lambda_0, \lambda_1, \lambda_2, \lambda_3] \quad i = 1, \dots, 6. \quad (\text{B.1})$$

To prove translational invariance we apply the substitutions given in Eq. (40) to g_j ($j = 1, \dots, 19$) which results in a new system of polynomials G_j forming the following ideal:

$$\mathcal{I}_T := \langle G_1, \dots, G_{19} \rangle \subseteq \mathbb{K}[c_i, d_i, \alpha, \beta, x_2, x_3, y_3, \lambda_0, \lambda_1, \lambda_2, \lambda_3] \quad i = 1, \dots, 6. \quad (\text{B.2})$$

It can be verified by the computational algebra software `Maple` that \mathcal{I} and \mathcal{I}_T are contained in each other, thus their varieties are identical.

To prove rotational invariance we apply the substitutions of Eq. (42) to g_j ($j = 1, \dots, 19$) which results in a new set of polynomials G_j forming the following ideal:

$$\mathcal{I}_R := \langle G_1, \dots, G_{19} \rangle \subseteq \mathbb{K}[c_i, d_i, e_0, e_1, x_2, x_3, y_3, \lambda_0, \lambda_1, \lambda_2, \lambda_3] \quad i = 1, \dots, 6. \quad (\text{B.3})$$

Again by the usage of the software `Maple`, it can be verified that \mathcal{I} is contained in \mathcal{I}_R and vice versa. The `Maple` files used for proving this lemma can be downloaded from [16]. \square

Note that in Lemma 3 we only get the invariance under Euclidean motions and not under equiform motions as in Lemma 1, because of the condition $E_B = 0$.

Appendix C. Explicit expressions for the distances of Theorem 1

The explicit expressions for the distances $D_{\star}^{\Delta}(\mathbf{K}, \mathbf{K}')$ with $\star \in \{\blacktriangle, \triangle\}$ read as follows:

$$D_{\blacktriangle}^{\Delta}(\mathbf{K}, \mathbf{K}') = \min \left[\frac{23}{630} (x_5^2 - x_5 x_6 + x_6^2 + y_6^2) \pm \frac{23}{630} (\text{sign}(\gamma) \sqrt{\eta}) \right] \quad (\text{C.1})$$

$$D_{\triangle}^{\Delta}(\mathbf{K}, \mathbf{K}') = \min \left[\frac{4}{15} (x_5^2 - x_5 x_6 + x_6^2 + y_6^2) \pm \frac{4}{15} (\text{sign}(\gamma) \sqrt{\eta}) \right] \quad (\text{C.2})$$

with

$$\eta := x_5^4 - 2x_5^3 x_6 + 3x_5^2 x_6^2 - x_5^2 y_6^2 - 2x_5 x_6^3 - 2x_5 x_6 y_6^2 + x_6^4 + 2x_6^2 y_6^2 + y_6^4, \quad (\text{C.3})$$

$$\gamma := e_0^2 x_5^2 y_6 + 2e_0^2 x_5 x_6 y_6 - 2e_0^2 x_6 y_6 - 2e_0^2 y_6^3 + 2e_0 e_1 x_5^3 - 6e_0 e_1 x_5^2 x_6 + 6e_0 e_1 x_5 x_6^2 + \quad (\text{C.4})$$

$$2e_0 e_1 x_5 y_6^2 - 4e_0 e_1 x_6^3 - 4e_0 e_1 x_6 y_6^2 - e_1^2 x_5^2 y_6 - 2e_1^2 x_5 x_6 y_6 + 2e_1^2 x_6^2 y_6 + 2e_1^2 y_6^3. \quad (\text{C.5})$$

This shows that the obtained values only depend on the geometry of the manipulator.